Atmos. Chem. Phys. Discuss., 15, 33675–33730, 2015
www.atmos-chem-phys-discuss.net/15/33675/2015/
doi:10.5194/acpd-15-33675-2015

Atmospheric Chemistry and Physics Discussions
Open Access
EGU

Optical properties of atmospheric fine particles near Beijing during the HOPE-J^{3}A Campaign

X. Xu[1,2,3], W. Zhao[1,2], Q. Zhang[1,2,3], S. Wang[1,2,3], B. Fang[1,2], W. Chen[5], D. S. Venables[6], X. Wang[7], W. Pu[8], X. Wang[8], X. Gao[1,2,4], and W. Zhang[1,2,4]

[1]Key Laboratory of Atmospheric Composition and Optical Radiation, Anhui Institute of Optics and Fine Mechanics, Chinese Academy of Sciences, Hefei, 230031, Anhui, China
[2]Laboratory of Atmospheric Physico-Chemistry, Anhui Institute of Optics and Fine Mechanics, Chinese Academy of Sciences, Hefei, 230031, Anhui, China
[3]Graduate School, University of Science and Technology of China, Hefei, 230026, Anhui, China
[4]School of Environmental Science and Optoelectronic Technology, University of Science and Technology of China, Hefei, 230026, Anhui, China
[5]Laboratoire de Physicochimie de l'Atmosphère, Université du Littoral Côte d'Opale, 59140 Dunkerque, France
[6]Department of Chemistry and Environmental Research Institute, University College Cork, Cork, Ireland
[7]Environment Research Institute, Shandong University, Jinan 250100, China

[8]Key Laboratory for Semi-Arid Climate Change of the Ministry of Education, College of Atmospheric Sciences, Lanzhou University, Lanzhou 730000, China

Received: 17 September 2015 – Accepted: 12 November 2015
– Published: 27 November 2015

Correspondence to: W. Zhao (wxzhao@aiofm.ac.cn)
and W. Zhang (wjzhang@aiofm.ac.cn)

Published by Copernicus Publications on behalf of the European Geosciences Union.

ACPD
15, 33675–33730, 2015

Abstract

The optical properties and chemical composition of $PM_{1.0}$ (particulate with an aerodynamic diameter of less than 1.0 µm) particles in a suburban environment (Huairou) near the mega-city Beijing were measured during the HOPE-J^{3}A (Haze Observation Project Especially for Jing-Jin-Ji Area) field campaign. The campaign covered the period November 2014 to January 2015 during the winter coal heating season. The average and standard deviations for the extinction, scattering, absorption coefficients, and the aerosol single scattering albedo (SSA) at $\lambda = 470$ nm during the measurement period were 201 ± 240, 164 ± 202, $37 \pm 43\,\mathrm{Mm}^{-1}$, and 0.80 ± 0.08, respectively. The mean mass scattering (MSE) and absorption (MAE) efficiencies were 4.77 ± 0.01 and $0.87 \pm 0.03\,\mathrm{m}^2\mathrm{g}^{-1}$, respectively. Highly time-resolved air pollution episodes clearly show the dramatic evolution of the $PM_{1.0}$ size distribution, extensive optical properties (extinction, scattering, and absorption coefficients) and intensive optical properties (single scattering albedo and complex refractive index) during haze formation, development and decline. Time periods were classified into three different pollution levels (clear, slightly polluted, and polluted) for further analysis. It was found that: (1) The diurnal patterns of the aerosol extinction, scattering, absorption coefficients, and SSA differed for the three pollution classes. (2) The real and imaginary part of complex refractive index (CRI) increased, while the SSA decreased from clear to polluted days. (3) The relative contributions of organic and inorganic species to observed aerosol composition changed significantly from clear to polluted days: the organic mass fraction decreased (50 to 43 %) while the proportion of sulfates, nitrates, and ammonium increased strongly (34 to 44 %). (4) The fractional contribution of chemical components to extinction coefficients was calculated by using the modified IMPROVE algorithm. Organic mass was the largest contributor (58 %) to the total extinction of $PM_{1.0}$. When the air quality deteriorated, the change of the relative contribution of sulfate aerosol to the total extinction was small, but the contribution of nitrate aerosol increased significantly (from 17 % on clear days to 23 % on polluted days). (5) The observed mass scatter-

ACPD
15, 33675–33730, 2015

ing efficiencies increased consistently with the pollution extent, however, the observed mass absorption efficiencies increased consistently with increasing mass concentration in slightly pollution conditions, but decreased under polluted conditions.

1 Introduction

Atmospheric aerosols have significant effects on climate forcing (Ramanthan et al., 2001; Anderson et al., 2003; Bahadur et al., 2012), environment (Cao et al., 2013; Huang et al., 2014), and human health (Nel, 2005; S. Zheng et al., 2015). Visibility is regarded as an indicator of air quality, which is mostly reduced by the scattering and absorption of solar light by fine particles (Watson, 2002). Uncertainties in atmospheric visibility are mainly due to the uncertainties associated with the aerosols' optical properties, which are closely related to the physical and chemical properties of atmospheric aerosol (including chemical components, size distribution, mixing state, morphology and hygroscopic properties). Understanding how the physical and chemical characteristics affect the optical properties of the atmospheric aerosol is key to improve quantitative estimates of direct radiative forcing and to determine the environmental effects of particles. To ascertain the relationships between these parameters, many research campaigns have been performed during the past decade, such as ACE-1 (Bates et al., 1998), ACE-2 (Raes et al., 2000), INDOEX (Eldering, 2002), ACE-Asia (Quinn, 2004; Doherty et al., 2005), PRIDE-PRD2004 (Zhang et al., 2008), MILAGRO (Marley et al., 2009), CAREBeijing (Jung et al., 2009; Garland et al., 2009; Wu et al., 2011) and CalNex campaign (Cahill et al., 2012; Thompson et al., 2012; Ryerson et al., 2013; X. Zhang et al., 2013).

Rapid urbanization and economic development has brought about serious environmental problems in the megacities of China (Han et al., 2015). The North China Plain (NCP) region in northeast China has one of the highest global aerosol concentrations (Sun et al., 2013) due to the dense population, a large number of mobile vehicles and the great industrial activity. The China National Ambient Air Quality Standard des-

ACPD
15, 33675–33730, 2015

ignates a daily average concentration of $PM_{2.5}$ greater than 75 $\mu g\,m^{-3}$ as harmful to health. However, $PM_{2.5}$ concentrations in China often grossly exceed this limit – for instance, reported daily average mass concentration of $PM_{2.5}$ in January 2013 were higher than 500 $\mu g\,m^{-3}$ (Andersson et al., 2015). A large amount of atmospheric pollutants are emitted from fossil fuel, biomass burning and urban construction (Lei et al., 2011; Zhang et al., 2011). The complex mixtures of various pollutant sources has resulted in a highly complex nature of aerosol physical, chemical and optical properties.

In recent years, many campaigns have been conducted in Beijing to study the relationships between the mass concentrations, optical properties, chemical components, hygroscopic properties, mixing state, new particle formation, light apportionment and meteorological conditions (Liu et al., 2013; Sun et al., 2013, 2015; Guo et al., 2014; Andersson et al., 2015; Han et al., 2015; Wang et al., 2015; Wu et al., 2015; Xu et al., 2011; X. J. Zhao et al., 2013; G. J. Zheng et al., 2015). It is worth noting that atmospheric dynamic processes differ between polluted and cleaner periods and that secondary aerosols were suggested to be the major contributor to haze formation (Quan et al., 2014; Y. L. Sun et al., 2014). Research in the Pearl River Delta of China has shown that submicron particles contribute more than 90 % of the particle extinction (Cheng et al., 2008). However, few studies in the NCP region have focused on light extinction contribution of submicron aerosol under different air pollution conditions. And the evolution of the intensive optical properties (complex refractive index, CRI, and single scattering albedo, SSA, ω, the ratio of scattering to extinction) in haze formation, development and decline were rarely reported. Comprehensive studies of intensive optical properties and light apportionment are necessary for a better understanding of the evolution of aerosol physical and optical properties in the NCP.

In this paper, we report continuous measurements of the optical properties, particle size distributions, and chemical components of the submicron aerosol at a suburban site (Huairou) from 16 November 2014 to 11 January 2015. The CRI for $PM_{1.0}$ particles were retrieved with Mie theory by treating the submicron aerosols as homogeneous spherical particles. The fractional contribution of aerosol chemical components to the

ACPD
15, 33675–33730, 2015

aerosol total extinction coefficient were calculated by the modified IMPROVE algorithm (Pitchford et al., 2007). The mass scattering and absorption efficiencies with respect to $PM_{1.0}$ mass concentrations were derived from particle size distribution measurements. $PM_{1.0}$ optical properties, chemical compositions, size distributions, chemical extinctions and mass scattering and absorption efficiencies were reported for three different pollution levels (clear, slight polluted, and polluted days). The results clearly showed that there was a large amount of light absorbing fine particles in Beijing in the winter time.

2 Experimental

The Haze Observation Project Especially for Jing-Jin-Ji (Beijing-Tianjin-Hebei, the national capital region of China) Area (HOPE-J^3A) field campaign took place at the Huairou campus of the University of Chinese Academy of Sciences (40°24′24.45″ N, 116°40′32.95″ E) from October 2014 to January 2015. The goal of the HOPE-J^3A campaign was to better understand the emissions, transport, and evolution of atmospheric fine particles and their precursors in the Jing-Jin-Ji area. Figure 1 shows the map of NCP and the average distribution of the MODIS (MODerate-resolution Imaging Spectroradiometer) AOD (aerosol optical depth) with a resolution of 0.2° × 0.2° during the field campaign from 16 November 2014 to 11 January 2015. The Huairou observation site (marked as a red star in Fig. 1) is situated about 60 km northeast of Beijing city center, and mainly surrounded by medium density residential suburban areas.

The instruments were installed on the 4th floor of Teaching Building 1, with the sample inlet about 2.5 m above the roof. The inlet consisted of a $PM_{1.0}$ ambient size cut (SF-$PM_{1.0}$, 1.0 $m^3 h^{-1}$, Seven Leekel Ingenieurburo GmbH), allowing only particles with an aerodynamic diameter smaller than 1 µm to enter the sampling line. Downstream of the aerosol inlet, a diffusion dryer was used to dry the sample aerosol below 15 % RH. The sample air was passed through a copper tube (6 m long with an inner diameter of 1 cm) at a flow rate of 38 L min^{-1}.

ACPD
15, 33675–33730, 2015

The particle size distribution between 14 and 662 nm was measured with a scanning mobility particle sizer (SMPS, TSI 3936), which comprised an electrostatic classifier (TSI 3080) and a condensation particle counter (TSI 3776). Diffusion losses and the effect of multicharged particles were corrected by the instrument software. The SMPS was calibrated with laboratory-generated, NIST traceable monodispersed polystyrene latex (PSL) spheres with diameters of 203 ± 5 nm (Thermo Scientific 3200A) and 296 ± 6 nm (Thermo Scientific 3300A) before and after the campaign (W. Zhao et al., 2013). The differences between the observed selected particle size and the certified diameter for the PSL spheres were within 2 %.

The optical properties of $PM_{1.0}$ particles were measured with a newly developed cavity-enhanced albedometer (Zhao et al., 2014). The albedometer, was based on a blue light-emitting-diode (LED) incoherent broadband cavity-enhanced absorption spectroscopy (IBBCEAS) system that incorporated an integrating sphere (IS). This instrument is a new tool for direct, in situ, and simultaneous measurement of aerosol scattering and extinction coefficients (and thus of the absorption coefficient and aerosol SSA, ω_{470}) at a mean wavelength of 470 nm. The advantage of broadband over single-wavelength measurements is its capacity to simultaneously measure multiple species present in the sample (gases and particles) using a single instrument. A spectral-fitting algorithm over the spectral range of 445–480 nm was applied to retrieve gas concentrations based on their spectral structure and thereby to remove the contribution of gas phase absorption from the aerosol extinction. The scattering signal was measured in the IS by a single channel photomultiplier tube (PMT), providing an integrated result over a narrow bandwidth of ~ 9 nm (full-width at half maximum, FWHM) in the spectral region of 465–474 nm. Truncation reduction tubes (Varma et al., 2003) were used to minimize the truncation angle to 1.2° for the forward and backward truncation angles. Based on a Mie scattering calculation, the truncated fraction of total scattering is about 0.22 % with this truncation angle for a 1 µm diameter spherical particle with a complex refractive index (CRI) of $m = 1.6 + i0$ at $\lambda = 470$ nm. This small truncation effect

ACPD
15, 33675–33730, 2015

was negligible in the context of the results we report here and no correction for the truncation underestimate was applied to our data.

The sample flow rate of the cavity-enhanced albedometer (the sample volume of the system was about 1.8 L) was 1.5 L min^{-1} at atmospheric pressure and the acquisition time for each measurement was 9 s (for a 1.5 s integrating time per spectrum, and six-spectra averaging). The temperature and relative humidity of the sample were measured with a hygrometer (Rotronic, model HC2 humidity sensor). The cavity was flushed with dry zero air every hour for acquisition of a reference spectrum. The reference spectrum was used both in the IBBCEAS retrieval (Fiedler et al., 2003) and to remove the contribution of light scattering from internal surfaces and Rayleigh scattering. The mirror reflectivity $R(\lambda)$ and the scaling factor (K') for the scattering channel of the albedometer were determined by He, N_2 and CO_2 every week. No deterioration of R and K' were observed during the campaign.

Another $PM_{1.0}$ sampler (SF-$PM_{1.0}$, Seven Leekel Ingenieurburo GmbH) was installed on the roof of the building (~ 20 m above the ground) to collect $PM_{1.0}$ samples with quartz filters (47 mm, MUNKTELL Corporation) for off-line aerosol chemical composition analysis. The flow rate was 38 L min^{-1} and samples were collected over the period of 16 November 2014 to 11 January 2015. The collection time period was 12 h: from 08:30 to 20:30 LT for daytime samples, and from 20:30 to 08:30 LT for nighttime samples. Before sampling, the quartz-fiber filters were preheated for 4 h at 600 °C in a muffle furnace, and ten filters were used as field blank samples in the sampling period. In total, 114 filters were collected; these were stored at −4 °C to prevent evaporation of volatilized species until they were analyzed.

A punch of 1.5 cm^2 was taken from each filter, and then heated in inert and oxidizing atmospheres to volatilize and combust the loaded carbon, respectively. The carbon (elemental carbon, EC, and organic carbon, OC) concentrations were determined with a thermal/optical transmittance aerosol carbon analyzer (Sunset Laboratory, Inc.) (NIOSH, 1996). The measurement principle and operation of the Sunset aerosol carbon analyzer was presented in a previous study (Peterson et al., 2002). Another punch

ACPD
15, 33675–33730, 2015

with a area of 2 cm^2 was taken from the rest of filter, extracted into 10 mL of deionized water (> 18 MΩ) via 20 min sonication, filtered using a 0.22 µm PTFE syringe filter, and stored in a refrigerator at 4 °C until chemical analysis. Eight water-soluble ion compositions [three anions: nitrate (NO_3^-), sulfate (SO_4^{2-}), chloride (Cl^-); five cations: ammonium (NH_4^+), sodium (Na^+), potassium (K^+), magnesium (Mg^{2+}) and calcium (Ca^{2+})] were determined by using Dionex ICS-90 Ion Chromatography with columns of AS14A and CS14A and eluents of $NaCO_3$-$NaHCO_3$ and methanesulfonic acid, respectively. Further details on this analysis are given elsewhere (Wang et al., 2013).

Meteorological parameters, including wind speed (WS) and direction (WD), temperature (T) and relative humidity (RH), were continuously recorded at the observation site. The mass concentration of $PM_{2.5}$ for the air quality classification was monitored by the National Environmental Bureau, and the data at Huairou were retrieved from the internet (http://113.108.142.147:20035/emcpublish/). In this work, the $PM_{2.5}$ pollution level was classified into three categories according to the technical regulation on Ambient Air Quality Index (on trial, HJ 633–2012) (http://kjs.mep.gov.cn/hjbhbz/bzwb/dqhjbh/jcgfffbz/201203/W020120410332725219541.pdf; A. Zhang et al., 2013; G. J. Zheng et al., 2015): clear day ($PM_{2.5}$ concentration $\leq 35\,\mu g\,m^{-3}$, when the corresponding individual air quality index (IAQI) ranged from 0 to 50), slightly polluted day ($35\,\mu g\,m^{-3} < PM_{2.5}$ concentration $\leq 115\,\mu g\,m^{-3}$, when IAQI ranged from 50 to 150), and polluted day ($115\,\mu g\,m^{-3} < PM_{2.5}$ concentration $\leq 350\,\mu g\,m^{-3}$, when IAQI ranged from 150 to 400). These pollution classes are usually based on $PM_{2.5}$ concentrations averaged from 00:00 to 23:59 on a specific date. For our filter samples, however, the collection time extended over two days; nevertheless, we apply the same categorization for our measurements from 20:30 (day 1) to 20:30 LT (day 2).

ACPD
15, 33675–33730, 2015

3 Optical data analysis method

3.1 Retrieval of aerosol complex refractive index

The scattering and extinction coefficients from particles are calculated based on (Pettersson et al., 2004):

$$\alpha_{\text{ep, sp}} = \int N(D_{\text{p}}) \frac{\pi}{4} D_{\text{p}}^2 Q_{\text{ext, scat}}(m, x) \mathrm{d}D_{\text{p}}, \tag{1}$$

where $x = \pi D_{\text{p}}/\lambda$ is the size parameter, $m = n + ik$ is the CRI of the particle (where n and k correspond to the real and imaginary parts of the CRI, respectively), N is the number of particles in the size bin $\mathrm{d}D_{\text{p}}$ with mean diameter D_{p} per unit volume, and $\frac{\pi}{4} D_{\text{p}}^2 Q_{\text{ext, scat}}(m, x)$ is the extinction or scattering cross section $\sigma_{\text{ep, sp}}$. The extinction or scattering efficiency, $Q_{\text{ext, scat}}$, is a function of the CRI, the morphology of the particles and the size parameter. For chemical homogeneous spherical particles, Q can be calculated from Mie theory.

The CRI is one of the intensive optical properties of atmospheric aerosols, and determined by the aerosols' size, shape, mixing state and chemical composition. Simultaneous measurement of the scattering and extinction coefficients by the cavity-enhanced albedometer provides a new approach for faster retrieval of the particulate CRI (Riziq et al., 2007; Mack et al., 2010; Zhao et al., 2014; X. Xu et al., 2015). The details of the CRI retrieval have been given in previous studies (Riziq et al., 2007; Mack et al., 2010). The measured extinction and scattering coefficients ($\alpha_{\text{ep,470}}$ and $\alpha_{\text{sp,470}}$) and the particle number size distribution, $N(D_{\text{p}})$, were used to determine the CRI. The real and imaginary parts of the CRI were varied (between 1.3 and 1.7 for the real part and between 0 and 0.1 for the imaginary part) to calculate the extinction and scattering coefficients for each size distribution. A set of refractive indices were determined by

ACPD
15, 33675–33730, 2015

finding the minimum of the "merit function", χ^2 (Mack et al., 2010):

$$\chi^2 = \frac{\left(\alpha_{\mathrm{ep}} - \alpha_{\mathrm{ep\_calc}}\right)^2}{\varepsilon^2_{\alpha_{\mathrm{ep}}}} + \frac{\left(\alpha_{\mathrm{sp}} - \alpha_{\mathrm{sp\_calc}}\right)^2}{\varepsilon^2_{\alpha_{\mathrm{sp}}}}. \tag{2}$$

Here, α_{ep} and α_{sp} are the measured values of the extinction and scattering coefficients, while $\alpha_{\mathrm{ep\_calc}}$ and $\alpha_{\mathrm{sp\_calc}}$ are the corresponding calculated values. $\varepsilon_{\alpha_{\mathrm{ep}}}$ and $\varepsilon_{\alpha_{\mathrm{sp}}}$ are the measurement uncertainty of α_{ep} and α_{sp}, respectively. The mean standard deviations of the extinction and scattering coefficients over 3 min were treated as the measurement uncertainty.

The values of n and k that satisfy $\chi^2 < \chi_0^2 + 2.298$, which fell within the 1σ error bound of the best measurement (with 68 % confidence level of χ^2 distribution), are considered acceptable. Projections of the contour lines (with a contour value of 2.298) on the n and k plane gave the standard errors Δn and Δk, respectively (Dinar et al., 2008; Zhao et al., 2014).

3.2 Chemical apportionment of aerosol optical properties

Chemical apportionment of light extinction of $PM_{1.0}$ was determined with a revised IMPROVE (Interagency Monitoring of Protected Visual Environments) algorithm (Pitchford et al., 2007). The IMPROVE algorithm is a simple method to estimate light extinction, which is based on multi-variable regression analysis. Light extinction can be estimated by multiplying the mass concentrations by the mass extinction efficient of each of seven major components: sulfate (assumed to be ammonium sulfate), nitrate (assumed to be ammonium nitrate), organic mass (OM, based on the measured mass concentration of organic carbon, OC), elemental carbon (EC), fine soil, sea salt (chlorine, Cl), and coarse mass (the differences between PM_{10} and $PM_{2.5}$ mass concentration).

ACPD
15, 33675–33730, 2015

The formulas for the reconstruction of aerosol extinction coefficient at $\lambda = 550\,\text{nm}$ can be expressed as following as (Pitchford et al., 2007):

$$\begin{aligned}\alpha_{\text{ext, 550 nm}} \approx\ & 2.2 \times f_s(\text{RH}) \times [\text{Small Sulfate}] + 4.8 \times f_L(\text{RH}) \times [\text{Large Sulfate}] \\ & + 2.4 \times f_s(\text{RH}) \times [\text{Small Nitrate}] + 5.1 \times f_L(\text{RH}) \times [\text{Large Nitrate}] \\ & + 2.8 \times [\text{Small Organic Mass}] + 6.1 \times [\text{Large Organic Mass}] \\ & + 10 \times [\text{Elemental Carbon}] + 1 \times [\text{Fine Soil}] \\ & + 1.7 \times f_{ss}(\text{RH}) \times [\text{Sea Salt}] + 0.6 \times [\text{Coarse Mass}] \\ & + \text{Rayleigh scattering (site specific)} + 0.33 \times [\text{NO}_2\,(\text{ppb})].\end{aligned} \tag{3}$$

The large and small parts are defined by the IMPROVE formula as (Pitchford et al., 2007; Cao et al., 2012):

$$\begin{aligned}&[\text{Large X}] = [\text{Total X}]^2/20, \text{ for } [\text{Total X}] < 20\,\mu\text{g}\,\text{m}^{-3} \\ &[\text{Large X}] = [\text{Total X}], \text{ for } [\text{Total X}] \geq 20\,\mu\text{g}\,\text{m}^{-3} \\ &[\text{Small X}] = [\text{Total X}] - [\text{Large X}]\end{aligned} \tag{4}$$

where X = sulfate, nitrate or OM. The concentration of ammonium sulfate ($[(NH_4)_2SO_4]$) was 1.375 times the sulfate concentration ($[SO_4^{2-}]$), and the ammonium nitrate ($[NH_4NO_3]$) was 1.29 times the nitrate concentrations ($[NO_3^-]$). OM concentration was estimated by multiplying the reported OC concentration by a factor of 1.6 (Turpin and Lim, 2001). The mass extinction efficiency of $10\,\text{m}^2\,\text{g}^{-1}$ (Watson, 2002; Pitchford et al., 2007; Cao et al., 2012; Han, 2014) to EC concentration was employed to calculate $\alpha_{\text{ep,550}}$.

One point should be kept in mind that the above discussion of the IMPROVE algorithm was suitable for the reconstruction of atmospheric aerosol extinction at $\lambda = 550\,\text{nm}$. In this study, the optical properties of $PM_{1.0}$ were measured at $\lambda = 470\,\text{nm}$. The IMPROVE algorithm need further improve to well represent the chemical apportionment of light extinction for $PM_{1.0}$ particles. Since dry $PM_{1.0}$ aerosols were measured, the coarse mass and the hygroscopic increase of inorganic component were

ACPD
15, 33675–33730, 2015

ignored for the inputs of the IMPROVE algorithm. The fine soil component was also left out in apportioning the extinction coefficient due to its very small fraction in $PM_{1.0}$ particles during wintertime in Beijing (K. Sun et al., 2014). The dry mass extinction efficiencies for ammonium sulfate, ammonium nitrate and OM at $\lambda = 470$ nm were calculated by using the Mie theory and were compared with that values at $\lambda = 550$ nm (Please find out more information in the Supplement Sect. S1). The mass extinction efficiencies of inorganic mass (including sulfate, nitrate and sea salt), organic mass, and element carbon for the input of the IMPROVE formula at $\lambda = 470$ nm should be multiplied by a scale factor of 1.31, 1.30 and 1.08, respectively. The modified IMPROVE function for $PM_{1.0}$ extinction at $\lambda = 470$ nm could be rewritten as following:

$$\begin{aligned}\alpha_{\text{ext, 470 nm, PM}_{1.0}} \approx\ & 2.88 \times [\text{Small Sulfate}] + 6.29 \times [\text{Large Sulfate}] \\ & + 3.14 \times [\text{Small Nitrate}] + 6.68 \times [\text{Large Nitrate}] \\ & + 3.64 \times [\text{Small Organic Mass}] + 7.93 \times [\text{Large Organic Mass}] \\ & + 10.8 \times [\text{Elemental Carbon}] + 2.23 \times [\text{Sea Salt}].\end{aligned} \tag{5}$$

3.3 Mass scattering and absorption efficiencies

Mass scattering (MSE) and absorption (MAE) efficiencies are the key parameters in climate and chemical transport models for estimating radiative forcing and apportioning chemical extinction budgets (Bates et al., 2006; Malm and Hand, 2007). MSE and MAE are defined as the ratio of the light scattering and absorption coefficients to the aerosol mass concentration, respectively. Knowledge of the MSEs and MAEs of each components of atmospheric aerosol is helpful for accurate source apportionment and used for estimating radiative forcing in climate modes. Two methods are used in the literature to obtain the MSEs and MAEs of individual components: multiple linear regression of measured scattering and absorption coefficients against mass concentrations of individual components (Malm and Hand, 2007; Tao et al., 2014b), and application of a Mie

ACPD
15, 33675–33730, 2015

algorithm based on measured chemical and volume size distributions and an assumed complex refractive index (Cheng et al., 2008, 2015).

In this study, data on the size-resolved chemical component was not available and individual chemical components were sampled with poor time resolution (12 h sample^{-1}). Therefore, the observed MSEs and MAEs were obtained based on the linear regression of the measured values of $\alpha_{sp,470}$ and $\alpha_{ap,470}$ against the mass concentrations of $PM_{1.0}$. The $PM_{1.0}$ mass concentrations were determined by multiplying the volume concentrations (calculated by the measured number size distribution) by the average mass density (calculated by the volume weighted method) (Hasan and Dzubay, 1983), where the fractions of five major contributing components (ammonium sulfate, ammonium nitrate, organic mass, element carbon and sea salt) to the $PM_{1.0}$ composition were considered.

4 Results and discussion

An overview of the measurement results of the aerosol optical properties, size distribution, and chemical composition of $PM_{1.0}$ particles is shown in Table 1 and Fig. 2. During the campaign, the measured aerosol extinction ($\alpha_{ep,470}$), scattering ($\alpha_{sp,470}$), and absorption coefficient ($\alpha_{ap,470}$) ranged from 0.6–1165, 0.1–1150 and 0–276 Mm^{-1}, respectively. The time profiles of these properties also showed several periods during which the particle concentration would steadily build up, before rapid dissipation and return to fewer and smaller particles.

We present our results as follows: Firstly, a selected air pollution episode will be investigated in detail for clearly showing the haze formation, development and decline. The extensive optical properties (extinction, scattering, and absorption coefficients) and intensive optical properties (SSA and CRI) will be given during this period. Secondly, the diurnal variations of aerosol size distribution, optical properties and chemical composition on different pollution days during the campaign will be considered. Thirdly, chemical apportionment of aerosol extinction will be studied based on the modified IM-

ACPD
15, 33675–33730, 2015

PROVE algorithm. And finally, the MSE and MAE of $PM_{1.0}$ particles for clear, slightly polluted, and polluted days will be given.

4.1 Temporal variations of optical properties during a selected air pollution episode

The temporal variations of aerosol particle number and surface size distribution, aerosol extinction, scattering, absorption coefficients, ω_{470}, and the retrieved CRIs from 22 to 24 November 2014 are presented in Fig. 3. The corresponding temporal wind direction and speed, temperature, relative humidity and pressure of atmosphere air are shown in the upper panel of Fig. 4. The time series of $PM_{1.0}$ particle number distribution during the episode varied with the meteorological conditions and the sources of pollutants. To emphasize the variation of these parameters during the episode, the extended air pollution episode was divided into six shorter periods. The statistical analyses of these periods are summarized in Table 2.

A 24 h back trajectories starting at 200 m a.g.l. in Huairou site calculated every 6 h (at 00:00, 6:00, 12:00 and 18:00 LT) are shown in the lower panel of Fig. 4 (http://ready.arl.noaa.gov/HYSPLIT.php). The clusters of 1–2 and 8–10 were from the northerly direction, with clean air masses, high transport height and long transport pathway. The clusters 3–7 are mainly from the southerly direction, with polluted air masses, low transport height and short transport pathway.

For Period 1, the trajectory indicated that the air masses came from the north with clean air, and carried pollutants from northeast areas to the observation site, with concentrations of small size and high light absorption particles increasing. For Period 2, the air masses came from the north with clean air, but reduced height led to bring surface aerosols to observation site. Strong wind did not favour accumulation of pollutants but promoted new particle formation. For Periods 3 and 4, the trajectory indicated that the pollutants came from the south, resulting in the accumulation of the pollution. Furthermore, the shorter transport pathway of air masses suggested that the composition was dominated by local emissions, including primary emissions and secondary

ACPD
15, 33675–33730, 2015

formation. For Period 5, cluster 7 indicates that the airflow started over the Beijing city area and passed over the southwestern direction of the observation site. Air masses following this short path would bring surface air pollutants to Huairou site, attributing to the formation of serious haze.

Period 1: First traffic-dominated pollution period (05:40–10:00 LT 22 November)

Relatively small, light absorbing particles dominated during this period. The mean diameter of the number size distribution was 56 ± 6 nm, and the average number and surface concentration were $2.1 \pm 0.8 \times 10^4$ particle cm^{-3} and $3.7 \pm 1.5 \times 10^8$ nm^2 cm^{-3}, respectively. The mean values of $\alpha_{ep,470}$, $\alpha_{sp,470}$, and $\alpha_{ap,470}$ were 56 ± 24, 44 ± 19 and 12 ± 6 Mm^{-1}, respectively. The ω_{470}, real and imaginary part of CRI (n, k) were 0.79 ± 0.03, 1.38 ± 0.06 and 0.03 ± 0.02, respectively. During the period, the winds were typically from the northeast; these clean air masses showed relatively large quantities of traffic emissions, with concentrations of small size and high light absorption particles increasing. Lower values of the SSA were found during this rush hour, in common with other studies that have similarly found minimum SSA values during the morning traffic rush hour (Garland et al., 2008; Lyamani et al., 2010).

Period 2: New particle formation period (12:40–15:00 LT 22 November)

This period started with clean atmospheric conditions and was characterized by the formation and growth of small particles. The mean diameter of the number size distribution was 25 ± 4 nm, and the mean values of $\alpha_{ep,470}$, $\alpha_{sp,470}$ and $\alpha_{ap,470}$ were 17 ± 5, 16 ± 5 and 1.0 ± 0.4 Mm^{-1}, respectively. The mean values of ω_{470}, n and k were 0.94 ± 0.03, 1.40 ± 0.06 and 0.008 ± 0.005, respectively. These values indicated that optical extinction in these newly formed particles was dominated by scattering, although it should be noted that the uncertainties in the ω_{470} were larger under these conditions of low scattering and extinction. Strong winds from northern directions transported clean and fresh air to Beijing, leading to sharply decreased pollutant levels, and promoting new particle

ACPD
15, 33675–33730, 2015

formation. Takegawa et al. (2009) showed that sulfate and organic matter accounted for the main components of newly formed Aitken mode particles. Guo et al. (2014) showed that the nucleation mode particles consisted of mainly secondary organics. These findings fitted with the results of retrieved intensive optical properties.

Period 3: Accumulated pollution period (15:30 LT 22 November–08:00 LT 23 November)

This period was characterized by the dominance of larger accumulation mode particles for several hours. The mean diameter of number and surface size distribution was 106 ± 16 and 229 ± 16 nm, respectively, which increased slowly from 15:30 LT (with a minimum value of 60 and 205 nm) to 21:40 LT (with a maximum value of 131 and 248 nm) except for a valley from 17:20–18:00 LT, which coincided with the afternoon rush hour. The mean values of $\alpha_{ep,470}$, $\alpha_{sp,470}$ and $\alpha_{ap,470}$ were 179 ± 69, 151 ± 57 and 28 ± 12 Mm^{-1}, respectively. In the first part of the period, the winds slowed down and turned to the south. This meteorology favored accumulation of local pollutants (including primary emissions and secondary productions) and transportation of pollutants from southern areas. Later on, the wind speed increased and the direction changed to the southeast. The accumulation of pollutants brought about the formation of haze. During the process, the number concentration increased about 1.7 times from 1.2×10^4 to 2.0×10^4 particle cm^{-3}, and the surface concentration increased about 1.3 times from 3.2×10^8 to 10.3×10^8 $nm^2\,cm^{-3}$, leading to large values of $\alpha_{ep,470}$ (285 Mm^{-1}), $\alpha_{sp,470}$ (235 Mm^{-1}) and $\alpha_{ap,470}$ (50 Mm^{-1}). The wind speed eventually decreased and the wind direction changed, first to northeastern, and then to southeastern directions. Another major peak in the extinction occurred during this period, when a large number of small size particles were observed. The mean values of ω_{470}, and the real part and imaginary part of CRI were 0.85 ± 0.01, 1.39 ± 0.04 and 0.02 ± 0.006, respectively. Clearly, the air masses from northeast areas carried larger numbers of small, light absorbing particles.

ACPD
15, 33675–33730, 2015

Period 4: Combined pollution period (08:30–12:00 LT 23 November)

Large numbers of small, light absorbing particles were produced during this period, which coincided with the morning rush hour. The mean diameter of the number and surface size distribution was 105 ± 16 and 251 ± 15 nm, respectively, and $\alpha_{ep,470}$, $\alpha_{sp,470}$ and $\alpha_{ap,470}$ were 405 ± 60, 321 ± 42 and $84 \pm 22\,Mm^{-1}$, respectively. The mean values of ω_{470} and the imaginary part of CRI were 0.79 ± 0.03 and 0.034 ± 0.008, respectively, which were similar to the values in the first traffic-dominated pollution period. However, the real part of the CRI (1.40 ± 0.03) was larger than that of the earlier traffic-dominated pollution period. During the period, weak winds from northern directions transported polluted air to the observation site leading to higher concentrations and a greater influence of emitted light absorbing particles. The accumulation of original and newly discharged primary pollutants led to sharp variations in the aerosol size distribution and extensive optical properties. Variations of the aerosol intensive optical properties were slight.

Period 5: Particle aggregation and removal period (12:30 LT 23 November–07:30 LT 24 November)

High extinction values were observed over this period, with a gradual increase and then decrease in extinction, scattering, and absorption. The mean values of $\alpha_{ep,470}$, $\alpha_{sp,470}$ and $\alpha_{ap,470}$ were 330 ± 110, 283 ± 94 and $46 \pm 16\,Mm^{-1}$, respectively. The mean values of ω_{470}, n and k were 0.86 ± 0.01, 1.44 ± 0.03, and 0.02 ± 0.01, respectively, which were both larger than the values of the period 4. In the first part of the period, winds from the north moderated and the wind direction then changed to the northeast, which favored accumulation of local pollutants. Later on, the wind changed to the southeast, with pollutants from the south contributing to the formation of serious haze. Particles dispersed later after the wind speed increased and its direction became northeastly. Both the mean diameter of the number and surface size distribution (124 ± 19 and

ACPD
15, 33675–33730, 2015

263 ± 11 nm) and n were larger in this period than in the other five periods. The light scattering efficiency increased with the increment of the particle size.

Period 6: Second traffic-dominated pollution period (08:00–11:10 LT 24 November)

This period corresponded to the morning rush hour on 24 November. The mean values of $\alpha_{ep,470}$, $\alpha_{sp,470}$ and $\alpha_{ap,470}$ were 80 ± 42, 64 ± 34 and 16 ± 8 Mm^{-1}, respectively, and were slightly larger than in the first traffic-dominated pollution period. The mean values of ω_{470} (0.78 ± 0.04), n and k (1.40 ± 0.04 and 0.04 ± 0.02) were comparable to the earlier traffic period. The mean diameter of the number and surface size distribution was 64 ± 12 and 226 ± 14 nm, respectively, and a larger n value was found. In this period, strong winds from the north transported clean air to the observation site, leading to lower particle concentrations and a higher influence of fresh local emissions.

According to the regulatory classification of the atmospheric pollution level, these six periods can be divided into two categories: clear day (22:00 LT 21 November–10:00 LT 22 November) and polluted day (10:00 LT 22 November–22:00 LT 22 November, 22:00 LT 22 November–10:00 LT 23 November, 10:00 LT 23 November–22:00 LT 23 November, 22:00 LT 23 November–10:00 LT 24 November). The mean fraction (deduced from Fig. 2d) of OM components contributing to the $PM_{1.0}$ decreased by 12 % (from 56 to 44 %), nitrate almost doubled in concentration (from 12 to 22 %), and sulfate slightly decreased (from 14 to 11 %) from clear to polluted days. It was suggested that inorganic species become more important during haze (Wang et al., 2015). The difference between sulfate and nitrate may be due to different mechanisms of the formation of sulfate and nitrate aerosols (G. J. Zheng et al., 2015).

In the selected haze episode, these six periods show dramatic variations in the $PM_{1.0}$ size distribution and the extensive optical properties of particles in the process of haze formation, development and decline. The evolution of intensive optical properties was related to the variation of $PM_{1.0}$ chemical components.

ACPD
15, 33675–33730, 2015

4.2 Variation of aerosol size distribution, optical properties and chemical composition on different air pollution days

Averages and standard deviations of the observed particle properties are summarized in Table 1 after grouping data into the different air quality classes. With increasing pollutant level, the extensive optical properties ($\alpha_{ep,470}$, $\alpha_{sp,470}$ and $\alpha_{ap,470}$) increased strongly as expected, whereas changes in the intensive optical properties (ω_{470}) were more modest. The measured $\alpha_{ep,470}$ and $\alpha_{sp,470}$ values sometimes exceeded 900 Mm^{-1}. There are obvious differences of the campaign average number size distribution of $PM_{1.0}$ under different pollution levels (cf. Fig. 3a). Compared with clear days, the effective mode diameter of particle number in the slightly polluted days was about 2 times larger, while the $PM_{1.0}$ extensive optical properties of extinction, scattering and absorption coefficients were respectively about 3.2, 3.2 and 3.3 times larger. However, the values of ω_{470} were similar (0.81 ± 0.10 for clear days and 0.79 ± 0.07 for slightly polluted days). There was no obvious correlation between extensive optical properties and wind direction (Fig. S2 in the Supplement). The contribution of SNA (sulfate, nitrate and ammonium) to the observed $PM_{1.0}$ mass concentration increased strongly on polluted vs. clear days (from 34 to 44 %). Similar trends were observed for $PM_{2.5}$ and NR-$PM_{1.0}$ during the January 2013 severe haze events in Beijing area (Y. L. Sun et al., 2014; Tao et al., 2015; G. J. Zheng et al., 2015). Huang et al. (2014) also reported higher levels of OM during pollution episodes and a combined SNA of about 38 %. The mean values of the extensive optical properties were much greater in polluted periods than in clean periods. The extinction, scattering and absorption coefficient increased by 9.7, 10.1 and 7.8 times, respectively, as the mass concentrations of light-scattering and light-absorbing species increased strongly from clean to polluted conditions. The contributions of ammonium nitrate to $PM_{1.0}$ light extinction increased by 7 % on polluted days, while the values of OM and EC both decreased by around 3 %. Thus, the SSA increased from 0.81 to 0.84, indicating a higher proportion of light-scattering components. These measurements therefore indicate that secondary inor-

ACPD
15, 33675–33730, 2015

ganic aerosol becomes more important during haze episodes (X. J. Zhao et al., 2013; Huang et al., 2014; G. J. Zheng et al., 2015).

Table 3 summarizes the extinction, scattering, absorption coefficients and SSA observed in this campaign and in other studies. The campaign average and standard deviation of $\alpha_{sp,470}$ was $166 \pm 199\,Mm^{-1}$, which was considerably higher than the value of $58 \pm 43\,Mm^{-1}$ (532 nm) of Pasadena (Thompson et al., 2012), and even higher than the urban site of Granada (Titos et al., 2012), and was comparable to the urban site of Guangzhou in China (Garland et al., 2008). Compared with other non-urban polluted sites in China, $\alpha_{sp,470}$ at Huairou was lower than Xinken ($333 \pm 137\,Mm^{-1}$) during October to November 2004 (Cheng et al., 2008), and it was lower than Yufa ($361 \pm 295\,Mm^{-1}$) during 11 August to 9 September 2006 (Garland et al., 2009), and it was about 2.9 times lower than Xianghe ($468 \pm 472\,Mm^{-1}$) in March 2005 (Li et al., 2007), while it was comparable to the result observed at Shangdianzi ($174 \pm 189\,Mm^{-1}$), an atmospheric background site, located ~ 150 km northeast of the urban center of Beijing (Yan et al., 2008). The average value of $\alpha_{ap,470}$ was $37 \pm 43\,Mm^{-1}$, which was comparable to Guangzhou, and 2.1 and 9.7 times higher than Shangdianzi and Pasadena, respectively. Moreover, the values $\alpha_{ap,470}$ was lower than other urban and suburban cities in China.

The regional difference in SSA can be considered in terms of the different sources of particles, including local primary emissions, transport emissions and secondary aerosol formations. Higher SSA values suggest a more mixed origin for particles, including industrial emissions, domestic coal combustion, and agricultural emissions. The average value of ω_{470} was 0.80 ± 0.08, which was lower than suburban sites in Xinken (0.83 ± 0.05), Xianghe (0.81–0.85) and Yufa (0.86 ± 0.07), and rural sites in Shangdianzi (0.88 ± 0.05), and Pasadena (0.92 ± 0.08), and comparable to an urban site in Beijing (0.80 ± 0.09) (He et al., 2009), but considerably higher than urban sites in Shanghai (0.70 ± 0.07) (Li et al., 2013) and Granada (0.71 ± 0.07) (Titos et al., 2012). The measured SSA value was similar to most urban/suburban/rural sites, but that some sites (Shanghai, Granada) have surprisingly low SSA values. These lower values of

ACPD
15, 33675–33730, 2015

SSA probably arose from higher contribution of vehicular emissions in Shanghai (Zhou et al., 2009), and both traffic emissions and a higher mass fraction of light absorbing particles caused by fuel-oil combustion in Granada (Titos et al., 2012).

4.2.1 Aerosol size distributions

Table 1 and Fig. 5a show the effective mode diameters and the mean size distributions under the three different pollution levels (clear, slightly polluted and polluted days). The effective mode diameters of particle number, surface and volume size distributions from mono-log normal fits to the measured submicron size distributions are given in Table 1 for the three classes of day. For clear and slightly polluted days, $D_{p,n}$ was within the size range of Aitken mode, whereas the value fell into the accumulation mode for polluted periods. However, $D_{p,s}$ and $D_{p,v}$ both fell in the range of accumulation mode under three pollution levels. For clear days, the mean particle number size distributions fitted by mono-log normal functions was around 41 nm, whereas a bimodal distribution was observed on slightly polluted and polluted days; modes were centered at 38 and 105 nm during slightly polluted periods, and at 38 and 151 nm for polluted periods. The mode of the number size distributions exhibits the expected displacement toward the accumulation mode with increasing levels of particulate matter.

4.2.2 Chemical composition

Table 1 and Fig. 5b show the mean values and the mean percentile compositions of observed chemical compositions of $PM_{1.0}$ particles under different pollution levels. With increasing pollution level, the SNA fraction increased by 10 %, while the EC and OM (1.6 times OC concentration) fractions decreased slightly. These values imply that the contribution of secondary inorganic aerosol to atmospheric fine aerosol increased during polluted periods, a finding that was consistent with previously reported on-line compositions in NR-PM_1 (Y. L. Sun et al., 2014) and $PM_{2.5}$ (G. J. Zheng et al., 2015) and off-line $PM_{2.5}$ samples (Huang et al., 2014; Tao et al., 2015; Yang et al., 2015). On

ACPD
15, 33675–33730, 2015

average, OM, nitrate, sulfate, ammonium, chloride and EC comprised 46.3, 18.0, 11.6, 10.3, 5.3 and 3.9 % of observed $PM_{1.0}$. The organic mass was the largest proportion in $PM_{1.0}$ particles, and the contribution of nitrate was larger than sulfate. Compared to summertime, the contribution of organics was significantly increased during wintertime, and primary organic aerosol dominated during the coal heating season (Sun et al., 2013). Huang et al. (2014) showed that the secondary organic aerosol (SOA) contributed 26 % of $PM_{2.5}$ in Beijing in January 2013 severe haze events, and indicated that the dominant effect of fossil SOA formation in Beijing regions. Compared to sulfate, the concentrations of nitrate and ammonium aerosol increased under high levels of pollution. The differences may be due to both photochemical and aqueous processing, which were important in the formation of nitrate (Wang et al., 2015), and aqueous processing may play a more important role in sulfate formation during wintertime (Sun et al., 2013).

4.2.3 Frequency distribution of optical properties

To summarize the observed results presented so far and to emphasize the differences in the optical properties among the three different pollution levels (clear, slightly polluted and polluted), the data are presented as histograms of the relative frequency of occurrence of $\alpha_{ep,470}$, $\alpha_{sp,470}$, $\alpha_{ap,470}$ and ω_{470} (Fig. 6). Approximately 71 % of extinction and scattering coefficients values were lower than 200 Mm^{-1}, and nearly 80 % of absorption coefficient values were located in the range of 1.5–50 Mm^{-1}. Approximately 90 % of the ω_{470} values fell into the range of 0.70–0.97. The average values of $\alpha_{ep,470}$, $\alpha_{sp,470}$, $\alpha_{ap,470}$ increased under high pollution levels. The frequency distributions of extensive optical parameters were not normal distributions, reflecting the rough classification of the pollution level based on 24 h averages; this approach would include clean air periods during a polluted day, and vice versa. Compared with polluted days, the frequency distribution of the SSA showed similar patterns, and the average values were similar with clear and slightly polluted days.

ACPD
15, 33675–33730, 2015

4.2.4 Diurnal variations of aerosol optical properties

The diurnal variations of hourly averaged extinction, scattering, absorption coefficient and SSA on clear, slightly polluted and polluted days are presented in Fig. 7. Broadly similar patterns were observed for the extensive optical properties for different pollutant levels. Extinction ($\alpha_{ep,470}$) and scattering ($\alpha_{sp,470}$) tended to be lower during daytime and higher at night. These patterns are consistent with the expected diurnal behavior of the boundary layer height, where vertical mixing and higher boundary layer heights during the day diluted the particles and hence reduced $\alpha_{ep,470}$ and $\alpha_{sp,470}$. At night, lowering of the boundary layer combined with continued emissions and accumulation of aerosol led to higher values of $\alpha_{ep,470}$ and $\alpha_{sp,470}$.

In addition to boundary layer effects, emissions associated with morning rush hour are apparent in the aerosol optical properties. $\alpha_{ep,470}$ and $\alpha_{sp,470}$ increased slowly in the morning (07:00–09:00 LT) to peak values at 09:00 LT, indicating significant emission and formation of particles during this period; these properties then decreased slowly until about 14:00 LT as the boundary height rose. The diurnal variation of $\alpha_{ap,470}$ had a similar pattern to $\alpha_{ep,470}$ and $\alpha_{sp,470}$, with two small peaks and valleys evident. However, the morning peak and subsequent valley occurred about 1 h earlier for $\alpha_{ap,470}$ compared to the scattering and extinction. Compared to clear and slightly polluted days, the morning rush hour maxima in $\alpha_{ep,470}$, $\alpha_{sp,470}$ and $\alpha_{ap,470}$ were notably later on polluted days, while the subsequent minima in these properties was earlier. These differences are likely due to differences in the boundary layer height under different pollution scenarios, where high pollutant levels would partially suppress convective mixing and result in lower boundary layer heights (Liu et al., 2013). The maximum values of $\alpha_{ap,470}$ occurred during the traffic rush hour and could be attributed to direct emissions of light absorbing species from vehicles. We note that the increase in $\alpha_{ap,470}$ from 06:00 to the maximum at 08:00 to 09:00 LT varies from 10 to 20 Mm^{-1}, a strikingly consistent increase given that there is an order of magnitude difference in $\alpha_{ap,470}$ for the different pollution days before this period. This observation suggests that the number and type

ACPD
15, 33675–33730, 2015

of particles are emitted during this time period is not strongly influenced by pollutant levels; this is very much what would be expected for morning traffic emissions. Compared with other studies (Garland et al., 2008; Han et al., 2014), the mean values of $\alpha_{ep,470}$, $\alpha_{sp,470}$ and $\alpha_{ap,470}$ are higher than the median values, indicating that a greater fluctuation of pollution conditions occurred at Huairou over the course of the campaign.

For clear and slightly polluted days, the diurnal cycle of ω_{470} displayed a dual-dip pattern. The first dip occurred at 10:00 LT in the morning, while the second minima was found in the evening 18:00 LT and 19:00 LT for clear and slightly polluted days, respectively. These lower ω_{470} values were consistent with emissions of strongly absorbing particles by vehicles over the morning and afternoon rush hours. A weaker dip in ω_{470} was also seen at 10:00 LT on polluted days; ω_{470} fluctuated around 0.84 after 12:00 LT, with no discernable pattern evident. The smaller changes in ω_{470} under polluted conditions reflect the relatively small contribution of a relatively constant amount of absorbing particulate matter to the high particle loads. In contrast, when such emissions form an appreciable part of the total aerosol load under clear or slightly polluted conditions, the changes in the SSA were marked.

During the campaign, the minimum hourly mean values of ω_{470} (0.767) occurred at 10:00 LT, while the peak values of $\alpha_{ep,470}$, $\alpha_{sp,470}$ and $\alpha_{ap,470}$ occurred at 09:00 LT. The delay was mainly due to lots of light absorption particles (e.g., black carbon) emitted during morning rush hour, while this was secondly caused by secondary aerosol formation. In Shanghai (Li et al., 2013) and Mexico City (Miranda et al., 2009), the daily minimum ω values also have a time delay with absorption peak in the morning traffic rush hour. The ω_{470} displays a high level between 02:00 and 04:00 LT and between 12:00 and 15:00 LT, mainly stemming from the increase of light scattering particles from secondary aerosol formation aging processes.

4.3 Chemical apportionment of aerosol optical properties

Over the past years, the chemical apportionment of α_{ep} or α_{sp} have been conducted in both urban and non-urban regions (Malm et al., 1994; Watson, 2002; Cheung et al.,

ACPD
15, 33675–33730, 2015

2005; Malm and Hand, 2007; Yang et al., 2007; Tao et al., 2009; Cao et al., 2012; Han et al., 2014; Tao et al., 2014a; Cheng et al., 2015). Commonly, ammonium sulfate was the largest contributor to $PM_{2.5}$ or PM_{10} α_{ep}, with a range from 20–50 %. However, fewer studies have been reported of the chemical contribution of different chemical components to the extinction of $PM_{1.0}$ under different pollution levels.

Studies in other Chinese megacities, such as Shanghai (Cheng et al., 2015) and Guangzhou (Tao et al., 2014b) and the data from US monitoring sites, shown that the revised IMPROVE algorithm underestimates the $PM_{2.5}$ extinction during high aerosol loading and overestimates the values under low aerosol loading. The underestimation and overestimation ratios in different studies are ranged from 11–26 % and 25–54 %, respectively (Cheng et al., 2015).

In this work, the reconstruction of $\alpha_{ep,470}$ of $PM_{1.0}$ particles was achieved by using the modified IMPROVE algorithm based on the measured concentrations of each composition (Fig. 8a), which was well correlated with the measured $\alpha_{ep,470}$ ($R^2 = 0.96$) during this campaign (Fig. 8c). With improved mass extinction efficiencies, the agreement among the measured and calculated $PM_{1.0}$ extinction are good (with a slope of 1.04 ± 0.04) when the measured extinction coefficient was lower than 300 Mm^{-1} (as shown in the insert of Fig. 8c). When the observed extinction coefficients were larger than 300 Mm^{-1}, the reconstructed values by the modified IMPROVE algorithm were 16 % lower than observed values. The modified IMPROVE algorithm for $PM_{1.0}$ at $\lambda = 470$ nm well represent the chemical apportionment of light extinction. The reconstructed $PM_{1.0}$ mass concentration (Fig. 8b) using the modified IMPROVE algorithm was well correlated with the measured $PM_{1.0}$ mass concentration ($R^2 = 0.99$, slope = 1.00, intercept = 0.28) (Fig. 8d), indicating that the modified IMPROVE algorithm can be used to estimate the chemical apportionment for extinction in this campaign.

The average fractional contributions of each chemical component of dry $PM_{1.0}$ extinction coefficient with respect to different pollution levels are shown in Fig. 9. The optical extinction caused by OM, ammonium nitrate, ammonium sulfate, elemental car-

ACPD
15, 33675–33730, 2015

bon and sea salt accounted for 57.9, 17.8, 12.5, 8.6 and 3.2 % of the reconstructed $PM_{1.0}$ extinction in this campaign, respectively. The contribution of chemical compositions to aerosol extinction depends mainly on their mass concentrations. The mass concentrations of OM, ammonium nitrate, ammonium sulfate, element carbon and sea salt accounted for 50.4, 21.2, 16.8, 4.2 and 7.4 % of the reconstructed $PM_{1.0}$ mass concentrations, respectively. The organic constituents comprised a large fraction of $PM_{1.0}$ mass concentration, consistent with previous studies (Yao et al., 2010; Sun et al., 2013).

OM made the largest contribution to the extinction of $PM_{1.0}$ particles in this study. The relative contribution of OM (58 %) to the total extinction reported here was comparable to that previously reported in Beijing (54 %) during an extreme haze episode in January 2013 for $PM_{1.0}$ scattering (Wang et al., 2015), and in Shenzhen (45 %) in the winter of 2009 for $PM_{2.5}$ extinction (Yao et al., 2010). The contribution of organics was significantly increased during wintertime, and during the coal heating season in Beijing, the atmospheric particles were primary organic aerosol dominated (Sun et al., 2013). As there is a large number of mobile vehicles in the mega-cities of China, the vehicle emissions is also a large contributor to organic aerosol (Huang et al., 2012). From clear days to slightly polluted days, the relative contribution of organic mass to light extinction increased by 7 %, which may due to the increscent of the contribution of secondary organic aerosol (SOA) (Huang et al., 2014). The concentrations of nitrate and ammonium aerosol increased under high levels of pollution, the large formation of nitrate and ammonium resulted in the relative contribution of ammonium nitrate to $PM_{1.0}$ light extinction increased by 6.7 % (Wang et al., 2015).

Various anthropogenic emissions, especially coal consumption, biomass burning and vehicle exhaust, make the NCP is a region of significant source of EC. Although EC only comprised about 4 % of $PM_{1.0}$ mass concentration, however, as its highest absorption efficiency, which resulted in a rather higher contribution to $PM_{1.0}$ extinction. Under high aerosol loading conditions (high pollution levels), the relative contribution

ACPD
15, 33675–33730, 2015

of EC to the total light extinction was decreased, which was may due to the larger formation of secondary species in $PM_{1.0}$ particles.

4.4 Estimate of MSE and MAE of $PM_{1.0}$

Figure 10 shows the scattering and absorption coefficients plotted vs. mass concentrations for $PM_{1.0}$ under different pollution levels. The $PM_{1.0}$ mass concentrations were determined by multiplying the volume concentrations (calculated from the measured number size distribution) with the average mass density (calculated by the volume weighted method) (Hasan and Dzubay, 1983). The fraction of five major contributing components to the $PM_{1.0}$ composition were calculated using the IMPROVE algorithm. The densities of OM (1.4 $\mu g\,cm^{-3}$), ammonium nitrate (1.725 $\mu g\,cm^{-3}$), ammonium sulfate (1.748 $\mu g\,cm^{-3}$), elemental carbon (1.5 $\mu g\,cm^{-3}$) and sea salt (2.0 $\mu g\,cm^{-3}$) were based on literature values (Watson, 2002; Cheng et al., 2008). The average mass densities calculated by the volume-weighted method were 1.551, 1.557, 1.591 and 1.56 $g\,m^{-3}$ for clear, slightly polluted, polluted days and all campaign days, respectively.

The scattering and absorption coefficients were well correlated with the $PM_{1.0}$ mass concentrations. The derived $PM_{1.0}$ average mass scattering and absorption efficiency during the campaign were 4.77 ± 0.01 and $0.87 \pm 0.03\,m^2\,g^{-1}$, respectively (Fig. 10d). These values were comparable with the measurement results reported by Garland et al. (2008) in suburban Guangzhou in July 2006, where the $PM_{1.0}$ mass scattering and absorption efficiency calculated with assuming an average effective density of ammonium sulfate (1.7 $g\,cm^{-3}$) were 4.13 and 1.09 $m^2\,g^{-1}$, respectively. The reported MSE of $PM_{1.0}$ in this work was comparable to the value of $PM_{2.5}$ at $\lambda = 520$ nm obtained in urban Beijing (4.8 $m^2\,g^{-1}$) during wintertime (Tao et al., 2015), and higher than that obtained in Chengdu and Guangzhou (3.9 $m^2\,g^{-1}$) (Tao et al., 2014a, b). The scattering efficiency at Huairou was lower than that of Xinken (a non-urban polluted site), where $\sigma_{sp,PM_{1.0}}$ at 550 nm was $6.4 \pm 1.1\,m^2\,g^{-1}$ during October to November 2004 (Cheng et al., 2008). The derived mass extinction efficiency is $4.35 \pm 0.01\,m^2\,g^{-1}$, which

ACPD
15, 33675–33730, 2015

was comparable to the reported values during Aerosols 1999 (4.1–5.4 $m^2 g^{-1}$) (Quinn et al., 2001) and INDOEX 1999 (4.0–5.6 $m^2 g^{-1}$) (Quinn et al., 2002).

In this work, the MSE of $PM_{1.0}$ was 4.13 $m^2 g^{-1}$ during polluted days, which was 36 % higher than that during the slightly polluted days (3.04 $m^2 g^{-1}$) and 68 % higher than that during the clear days (2.45 $m^2 g^{-1}$) (Fig. 10a–c). The MSE of $PM_{1.0}$ was clearly increased with high concentration aerosol loading. Cheng et al. (2014) showed that the MSEs of ammonium nitrate, ammonium sulfate and organic matter increased rapidly with increasing mass concentration in the lower concentration condition, while the MSEs of ammonium nitrate and ammonium sulfate fluctuate in a narrow range at the higher concentration condition, when the MSE of organic matter is slightly smaller. One recent study (Tao et al., 2015) showed that the MSE was determined by the proportions of the dominant chemical components and their size distributions under different pollution levels. The MSEs in this work increase consistently with the mass concentration of particles, which is primarily due to having larger particles that scatter light more efficiently.

The observed MAEs were 0.64 ± 0.00, 0.87 ± 0.00 and 0.63 ± 0.01 $m^2 g^{-1}$ for clear, slightly polluted and polluted days, respectively. The MAE increased consistently with increasing mass concentration in slightly pollution conditions, but decreased under polluted conditions. At the same time, the EC fraction (the only absorber treated in IMPROVE algorithm) decreased with increasing pollution level. The increase of MAE under slightly polluted days suggested the formation of light absorption organic components (e.g. brown carbon).

The reconstructed extinction coefficients and mass concentrations (summation of the concentrations all 5 groups) by the modified IMPROVE algorithm were used to calculate the reconstructed MSEs and MAEs of $PM_{1.0}$ particles. The calculated MSEs were 1.59, 1.62 and 1.44 times larger than the observed MSEs for clear, slightly polluted and polluted days, respectively (Fig. 11a). But for all campaign days, the calculated value agree well with the measured result. However, contrary to the trends of MSE, the measured MAE values were 1.49, 1.58, 1.61 and 2.02 times larger than the calculated

ACPD
15, 33675–33730, 2015

values for clear, slightly polluted, polluted days, and all campaign days, respectively (Fig. 11b). The bias for MAEs clearly implied that light absorbing fine particles should be considered in the further work.

5 Summary and conclusions

$PM_{1.0}$ optical properties and composition at a suburban site near Beijing were measured as a part of the HOPE-J^{3}A campaign. The mean values of observed $\alpha_{ep,470}$ and $\alpha_{sp,470}$ were 201 ± 240 and $164 \pm 202\,Mm^{-1}$, respectively. The mean values of $\alpha_{ap,470}$ and ω_{470} were $37 \pm 43\,Mm^{-1}$ and 0.80 ± 0.08, respectively. In the measurement period, the extensive aerosol optical properties (extinction, scattering and absorption coefficients) were much more variable than the intensive properties (SSA and CRI).

Six periods were investigated in detail to study the evolution of intensive optical properties and chemical composition in $PM_{1.0}$ during an extended haze episode. For a traffic-dominated pollution period, winds from northern directions favored many small and light absorbing particles (e.g., black carbon) emitted during morning rush hour, leading to the lowest SSA and the highest imaginary component of the CRI. The highest values of ω_{470} (0.94 ± 0.03), and the lowest values of imaginary part of the CRI (0.008 ± 0.005) suggested that particles extinction in the new particle formation event is dominated by scattering particles. During the formation of haze, both the size and number concentration of atmospheric fine particles increased, which increased the light scattering efficiency and the real component of the CRI. For the combined pollution period, the accumulation of original and newly discharged primary pollutants led to sharply variations of the aerosol size distribution and extensive optical properties, and smaller variations of aerosol intensive optical properties. Moreover, the largest mean diameter and real part of CRI suggested that a larger number of secondary aerosols formation and growth during the aggregated and removal pollution event.

ACPD
15, 33675–33730, 2015

In Huairou site, the diurnal variations of $\alpha_{ep,470}$, $\alpha_{sp,470}$, and $\alpha_{ap,470}$ mainly depended on the diurnal variation of the boundary layer height, while primary emissions played an important role during the rush traffic hour. The local wind analysis showed some influence of wind speed on the extensive optical properties, but the relationships between intensive optical properties and wind direction were obscure.

Based on the modified IMPROVE algorithm, light extinction apportionment indicated that organic matter, ammonium nitrate, ammonium sulfate, element carbon and sea salt accounted for 58, 18, 12, 9 and 3 %, respectively. Organic matter was the largest contributor to the total extinction in $PM_{1.0}$. The calculated extinction agreed with the measured extinction coefficient and the correlation coefficient was 0.96, despite being based on a daily average chemical composition. From clean to polluted periods, the contribution of ammonium nitrate to $PM_{1.0}$ light extinction increased by 6.7 %, while the values of OM and EC decreased by 3.2 and 3.4 %, respectively. The result indicated that organic matter was the largest contributor to the total extinction in $PM_{1.0}$, and inorganic species became important during the polluted period in Huairou.

The observed MSEs of $PM_{1.0}$ were 2.45, 3.04 and 4.13 $m^2\,g^{-1}$ for clear, slightly polluted, and polluted days respectively. The MSE increased consistently with the pollution extent. Besides, the observed MAEs of $PM_{1.0}$ were 0.64, 0.72 and 0.63 $m^2\,g^{-1}$, respectively. The MAE increased consistently with increasing mass concentration in slightly pollution conditions, but decreased under polluted conditions. However, the EC fraction decreased with increasing pollution level, whereas the increase of MAE under slightly polluted days maybe due to the formation of other light absorption components (e.g. brown carbon).

In conclusion, our analysis reveals that the optical properties of aerosols change significantly during the evolution of haze. The new particle formation and primary emission was apparent on clear days. The newly formed particles were dominated by scattering components, with a high SSA of 0.94 ± 0.03 and imaginary part of CRI of 0.008 ± 0.005. Primary particles emitted during the rush hour were strongly light absorbing (e.g., black carbon), with a low SSA of 0.79 ± 0.03 and a high imaginary part of

ACPD
15, 33675–33730, 2015

CRI of 0.03 ± 0.006. The contents of sulfate, nitrate, and ammonium species were high during haze episodes; heterogeneous reactions become more important than photochemical reactions under these circumstances (G. J. Zheng et al., 2015), while the SSA was increased. It is also confirmed by the fact that the proportion of organic mass increased slightly, while inorganic compositions were apparently higher during the polluted periods than those under clean periods.

The Supplement related to this article is available online at doi:10.5194/acpd-15-33675-2015-supplement.

Acknowledgements. The authors wish thank to Zhouqing Xie at University of Science and Technology of China for providing the meteorological data used in this paper. This research was supported by the National Natural Science Foundation of China (41330424), the Natural Science Foundation of Anhui Province (1508085J03), the Key Research Program of the Chinese Academy of Sciences (KJZD-EW-TZ-G06–01), and the China Special Fund for Meteorological Research in the Public Interest (GYHY201406039). The support of the CaPPA project ("Chemical and Physical Properties of the Atmosphere"), funded by the French National Research Agency through the "Programme d'Investissement d'Avenir" (under contract ANR-10-LABX-005), is acknowledged.

References

Abo Riziq, A., Erlick, C., Dinar, E., and Rudich, Y.: Optical properties of absorbing and non-absorbing aerosols retrieved by cavity ring down (CRD) spectroscopy, Atmos. Chem. Phys., 7, 1523–1536, doi:10.5194/acp-7-1523-2007, 2007.

Anderson, T. L., Charlson, R. J., Schwartz, S. E., Knutti, R., Boucher, O., Rodhe, H., and Heintzenberg, J.: Atmospheric science. Climate forcing by aerosol – a hazy picture, Science, 300, 1103–1104, 2003.

Andersson, A., Deng, J., Du, K., Zheng, M., Yan, C., Skold, M., and Gustafsson, O.: Regionally-varying combustion sources of the January 2013 severe haze events over eastern China, Environ. Sci. Technol., 49, 2038–2043, doi:10.1021/es503855e, 2015.

Bahadur, R., Praveen, P. S., Xu, Y., and Ramanathan, V.: Solar absorption by elemental and brown carbon determined from spectral observations, P. Natl. Acad. Sci. USA, 109, 17366–17371, 2012.

Bates, T. S., Huebert, B. J., Gras, J. L., Griffiths, F. B., and Durkee, P. A.: International Global Atmospheric Chemistry (IGAC) project's first aerosol characterization experiment (ACE 1): overview, J. Geophys. Res., 103, 16297–16318, doi:10.1029/97jd03741, 1998.

Bates, T. S., Anderson, T. L., Baynard, T., Bond, T., Boucher, O., Carmichael, G., Clarke, A., Erlick, C., Guo, H., Horowitz, L., Howell, S., Kulkarni, S., Maring, H., McComiskey, A., Middlebrook, A., Noone, K., O'Dowd, C. D., Ogren, J., Penner, J., Quinn, P. K., Ravishankara, A. R., Savoie, D. L., Schwartz, S. E., Shinozuka, Y., Tang, Y., Weber, R. J., and Wu, Y.: Aerosol direct radiative effects over the northwest Atlantic, northwest Pacific, and North Indian Oceans: estimates based on in-situ chemical and optical measurements and chemical transport modeling, Atmos. Chem. Phys., 6, 1657–1732, doi:10.5194/acp-6-1657-2006, 2006.

Cahill, J. F., Suski, K., Seinfeld, J. H., Zaveri, R. A., and Prather, K. A.: The mixing state of carbonaceous aerosol particles in northern and southern California measured during CARES and CalNex 2010, Atmos. Chem. Phys., 12, 10989–11002, doi:10.5194/acp-12-10989-2012, 2012.

Cao, J., Chow, J. C., Lee, F. S. C., and Watson, J. G.: Evolution of $PM_{2.5}$ measurements and standards in the US and future perspectives for china, Aerosol Air Qual. Res., 13, 1197–1211, 2013.

Cao, J. J., Wang, Q. Y., Chow, J. C., Watson, J. G., Tie, X. X., Shen, Z. X., Wang, P., and An, Z. S.: Impacts of aerosol compositions on visibility impairment in Xi'an, China, Atmos. Environ., 59, 559–566, doi:10.1016/j.atmosenv.2012.05.036, 2012.

Cheng, Y. F., Wiedensohler, A., Eichler, H., Su, H., Gnauk, T., Brüggemann, E., Herrmann, H., Heintzenberg, J., Slanina, J., Tuch, T., Hu, M., and Zhang, Y. H.: Aerosol optical properties and related chemical apportionment at Xinken in Pearl River Delta of China, Atmos. Environ., 42, 6351–6372, doi:10.1016/j.atmosenv.2008.02.034, 2008.

Cheng, Z., Jiang, J., Chen, C., Gao, J., Wang, S., Watson, J. G., Wang, H., Deng, J., Wang, B., Zhou, M., Chow, J. C., Pitchford, M. L., and Hao, J.: Estimation of aerosol mass scattering ef-

ACPD
15, 33675–33730, 2015

ficiencies under high mass loading: case study for the megacity of Shanghai, China, Environ. Sci. Technol., 49, 831–838, doi:10.1021/es504567q, 2015.
Cheung, H. C., Wang, T., Baumann, K., and Guo, H.: Influence of regional pollution outflow on the concentrations of fine particulate matter and visibility in the coastal area of southern China, Atmos. Environ., 39, 6463–6474, doi:10.1016/j.atmosenv.2005.07.033, 2005.
Dinar, E., Abo Riziq, A., Spindler, C., Erlick, C., Kiss, G., and Rudich, Y.: The complex refractive index of atmospheric and model humic-like substances (HULIS) retrieved by a cavity ring down aerosol spectrometer (CRD-AS), Faraday Discuss., 137, 279–295, 2008.
Doherty, S. J., Quinn, P. K., Jefferson, A., Carrico, C. M., Anderson, T. L., and Hegg, D.: A comparison and summary of aerosol optical properties as observed in situ from aircraft, ship, and land during ACE-Asia, J. Geophys. Res., 110, D04201, doi:10.1029/2004jd004964, 2005.
Eldering, A., Ogren, J. A., Chowdhury, Z., Hughes, L. S., and Cass, G. R.: Aerosol optical properties during INDOEX based on measured aerosol particle size and composition, J. Geophys. Res., 107, 8001, doi:10.1029/2001jd001572, 2002.
Fiedler, S. E., Hese, A., and Ruth, A. A.: Incoherent broad-band cavity-enhanced absorption spectroscopy, Chem. Phys. Lett., 371, 284–294, 2003.
Gao, J., Wang, T., Zhou, X. H., Wu, W. S., and Wang, W. X.: Measurement of aerosol number size distributions in the Yangtze River delta in China: formation and growth of particles under polluted conditions, Atmos. Environ., 43, 829–836, doi:10.1016/j.atmosenv.2008.10.046, 2009.
Garland, R. M., Yang, H., Schmid, O., Rose, D., Nowak, A., Achtert, P., Wiedensohler, A., Takegawa, N., Kita, K., Miyazaki, Y., Kondo, Y., Hu, M., Shao, M., Zeng, L. M., Zhang, Y. H., Andreae, M. O., and Pöschl, U.: Aerosol optical properties in a rural environment near the mega-city Guangzhou, China: implications for regional air pollution, radiative forcing and remote sensing, Atmos. Chem. Phys., 8, 5161–5186, doi:10.5194/acp-8-5161-2008, 2008.
Garland, R. M., Schmid, O., Nowak, A., Achtert, P., Wiedensohler, A., Gunthe, S. S., Takegawa, N., Kita, K., Kondo, Y., Hu, M., Shao, M., Zeng, L. M., Zhu, T., Andreae, M. O., and Pöschl, U.: Aerosol optical properties observed during Campaign of Air Quality Research in Beijing 2006 (CAREBeijing-2006): characteristic differences between the inflow and outflow of Beijing city air, J. Geophys. Res., 114, D00g04, doi:10.1029/2008jd010780, 2009.
Guo, S., Hu, M., Zamora, M. L., Peng, J., Shang, D., Zheng, J., Du, Z., Wu, Z., Shao, M., Zeng, L., Molina, M. J., and Zhang, R.: Elucidating severe urban haze formation in China, P. Natl. Acad. Sci. USA, 111, 17373–17378, 2014.

ACPD
15, 33675–33730, 2015

Han, B., Zhang, R., Yang, W., Bai, Z., Ma, Z., and Zhang, W.: Heavy air pollution episodes in Beijing during January 2013: inorganic ion chemistry and source analysis using Highly Time-Resolved Measurements in an urban site, Atmos. Chem. Phys. Discuss., 15, 11111–11141, doi:10.5194/acpd-15-11111-2015, 2015.

Han, L., Zhou, W., and Li, W.: Increasing impact of urban fine particles ($PM_{2.5}$) on areas surrounding Chinese cities, Scientific Reports, 5, 12467, doi:10.1038/srep12467, 2015.

Han, T. T., Liu, X. G., Zhang, Y. H., Qu, Y., Gu, J. W., Ma, Q., Lu, K. D., Tian, H. Z., Chen, J., Zeng, L. M., Hu, M., and Zhu, T.: Characteristics of aerosol optical properties and their chemical apportionments during CAREBeijing 2006, Aerosol Air Qual. Res., 14, 1431–1442, 2014.

Hasan, H. and Dzubay, T. G.: Apportioning light extinction coefficients to chemical species in atmospheric aerosol, Atmos. Environ., 17, 1573–1581, 1983.

He, X., Li, C. C., Lau, A. K. H., Deng, Z. Z., Mao, J. T., Wang, M. H., and Liu, X. Y.: An intensive study of aerosol optical properties in Beijing urban area, Atmos. Chem. Phys., 9, 8903–8915, doi:10.5194/acp-9-8903-2009, 2009.

Huang, R. J., Zhang, Y., Bozzetti, C., Ho, K.-F., Cao, J., Han, Y., Dällenbach, K. R., Slowik, J. G., Platt, S. M., Canonaco, F., Zotter, P., Wolf, R., Pieber, S. M., Bruns, E. A., Crippa, M., Ciarelli, G., Piazzalunga, A., Schwikowski, M., Abbaszade, G., Schnelle-Kreis, J., Zimmermann, R., An, Z., Szidat, S., Baltensperger, U., Haddad, I. E., and Prévôt, A. S. H.: High secondary aerosol contribution to particulate pollution during haze events in China, Nature, 514, 218–222, 2014.

Jung, J., Lee, H., Kim, Y. J., Liu, X. G., Zhang, Y. H., Hu, M., and Sugimoto, N.: Optical properties of atmospheric aerosols obtained by in situ and remote measurements during 2006 Campaign of Air Quality Research in Beijing (CAREBeijing-2006), J. Geophys. Res., 114, D00g02, doi:10.1029/2008jd010337, 2009.

Lei, Y., Zhang, Q., He, K. B., and Streets, D. G.: Primary anthropogenic aerosol emission trends for China, 1990–2005, Atmos. Chem. Phys., 11, 931–954, doi:10.5194/acp-11-931-2011, 2011.

Li, C., Marufu, L. T., Dickerson, R. R., Li, Z., Wen, T., Wang, Y., Wang, P., Chen, H., and Stehr, J. W.: In situ measurements of trace gases and aerosol optical properties at a rural site in northern China during East Asian Study of Tropospheric Aerosols: an international regional experiment 2005, J. Geophys. Res., 112, D22S04, doi:10.1029/2006jd007592, 2007.

ACPD
15, 33675–33730, 2015

Li, L., Chen, J. M., Wang, L., Melluki, W., and Zhou, H. R.: Aerosol single scattering albedo affected by chemical composition: an investigation using CRDS combined with MARGA, Atmos. Res., 124, 149–157, doi:10.1016/j.atmosres.2012.11.007, 2013.

Liu, X. G., Li, J., Qu, Y., Han, T., Hou, L., Gu, J., Chen, C., Yang, Y., Liu, X., Yang, T., Zhang, Y., Tian, H., and Hu, M.: Formation and evolution mechanism of regional haze: a case study in the megacity Beijing, China, Atmos. Chem. Phys., 13, 4501–4514, doi:10.5194/acp-13-4501-2013, 2013.

Lyamani, H., Olmo, F. J., and Alados-Arboledas, L.: Physical and optical properties of aerosols over an urban location in Spain: seasonal and diurnal variability, Atmos. Chem. Phys., 10, 239–254, doi:10.5194/acp-10-239-2010, 2010.

Mack, L. A., Levin, E. J. T., Kreidenweis, S. M., Obrist, D., Moosmüller, H., Lewis, K. A., Arnott, W. P., McMeeking, G. R., Sullivan, A. P., Wold, C. E., Hao, W.-M., Collett Jr., J. L., and Malm, W. C.: Optical closure experiments for biomass smoke aerosols, Atmos. Chem. Phys., 10, 9017–9026, doi:10.5194/acp-10-9017-2010, 2010.

Malm, W. C. and Hand, J. L.: An examination of the physical and optical properties of aerosols collected in the IMPROVE program, Atmos. Environ., 41, 3407–3427, doi:10.1016/j.atmosenv.2006.12.012, 2007.

Malm, W. C., Sisler, J. F., Huffman, D., Eldred, R. A., and Cahill, T. A.: Spatial and seasonal trends in particle concentration and optical extinction in the United States, J. Geophys. Res., 99, 1347–1370, doi:10.1029/93jd02916, 1994.

Marley, N. A., Gaffney, J. S., Castro, T., Salcido, A., and Frederick, J.: Measurements of aerosol absorption and scattering in the Mexico City Metropolitan Area during the MILAGRO field campaign: a comparison of results from the T0 and T1 sites, Atmos. Chem. Phys., 9, 189–206, doi:10.5194/acp-9-189-2009, 2009.

Nel, A.: Atmosphere. Air pollution-related illness: effects of particles, Science, 308, 804–806, 2005.

Paredes-Miranda, G., Arnott, W. P., Jimenez, J. L., Aiken, A. C., Gaffney, J. S., and Marley, N. A.: Primary and secondary contributions to aerosol light scattering and absorption in Mexico City during the MILAGRO 2006 campaign, Atmos. Chem. Phys., 9, 3721–3730, doi:10.5194/acp-9-3721-2009, 2009.

Peterson, M. R. and Richards, M. H.: Thermal-optical-transmittance analysis for organic, elemental, carbonate, total carbon, and OCX2 in $PM_{2.5}$ by the EPA/NIOSH method, in: Proceedings, Symposium on Air Quality Measurement Methods and Technology-2002, San Fran-

ACPD
15, 33675–33730, 2015

cisco, California, 13–15 November 2002, edited by: Winegar, E. D. and Tropp, R. J., Air and Waste Management Association, Pittsburgh, PA, 83-1–83-19, 2002.
Pettersson, A., Lovejoy, E. R., Brock, C. A., Brown, S. S., and Ravishankara, A. R.: Measurement of aerosol optical extinction at with pulsed cavity ring down spectroscopy, J. Aerosol Sci., 35, 995–1011, 2004.
Pitchford, M., Malm, W., Schichtel, B., Kumar, N., Lowenthal, D., and Hand, J.: Revised algorithm for estimating light extinction from IMPROVE particle speciation data, J. Air Waste Manage., 57, 1326–1336, doi:10.3155/1047-3289.57.11.1326, 2007.
Quan, J. N., Tie, X., Zhang, Q., Liu, Q., Li, X., Gao, Y., and Zhao, D. L.: Characteristics of heavy aerosol pollution during the 2012–2013 winter in Beijing, China, Atmos. Environ., 88, 83–89, doi:10.1016/j.atmosenv.2014.01.058, 2014.
Quinn, P. K.: Aerosol optical properties measured on board the Ronald H. Brownduring ACE-Asia as a function of aerosol chemical composition and source region, J. Geophys. Res.-Atmos, 109, D19S01, doi:10.1029/2003JD004010, 2004.
Quinn, P. K., Coffman, D. J., Bates, T. S., Miller, T. L., Johnson, J. E., Voss, K., Welton, E. J., and Neususs, C.: Dominant aerosol chemical components and their contribution to extinction during the aerosols cruise across the Atlantic, J. Geophys. Res.-Atmos, 106, 20783–20809, doi:10.1029/2000jd900577, 2001.
Quinn, P. K., Coffman, D. J., Bates, T. S., Miller, T. L., Johnson, J. E., Welton, E. J., Neususs, C., Miller, M., and Sheridan, P. J.: Aerosol optical properties during INDOEX 1999: means, variability, and controlling factors, J. Geophys. Res.-Atmos, 107, 8020, doi:10.1029/2000jd000037, 2002.
Raes, F., Bates, T., McGovern, F., and Van Liedekerke, M.: The 2nd Aerosol Characterization Experiment (ACE-2): general overview and main results, Tellus B, 52, 111–125, doi:10.1034/j.1600-0889.2000.00124.x, 2000.
Ramanathan, V., Crutzen, P. J., Kiehl, J. T., and Rosenfeld, D.: Aerosols, climate, and the hydrological cycle, Science, 294, 2119–2124, 2001.
Ryerson, T. B., Andrews, A. E., Angevine, W. M., Bates, T. S., Brock, C. A., Cairns, B., Cohen, R. C., Cooper, O. R., de Gouw, J. A., Fehsenfeld, F. C., Ferrare, R. A., Fischer, M. L., Flagan, R. C., Goldstein, A. H., Hair, J. W., Hardesty, R. M., Hostetler, C. A., Jimenez, J. L., Langford, A. O., McCauley, E., McKeen, S. A., Molina, L. T., Nenes, A., Oltmans, S. J., Parrish, D. D., Pederson, J. R., Pierce, R. B., Prather, K., Quinn, P. K., Seinfeld, J. H., Senff, C. J., Sorooshian, A., Stutz, J., Surratt, J. D., Trainer, M., Volkamer, R., Williams, E. J.,

ACPD
15, 33675–33730, 2015

and Wofsy, S. C.: The 2010 California Research at the Nexus of Air Quality and Climate Change (CalNex) field study, J. Geophys. Res., 118, 5830–5866, doi:10.1002/Jgrd.50331, 2013.

Sun, K., Qu, Y., Wu, Q., Han, T. T., Gu, J. W., Zhao, J. J., Sun, Y. L., Jiang, Q., Gao, Z. Q., Hu, M., Zhang, Y. H., Lu, K. D., Nordmann, S., Cheng, Y. F., Hou, L., Ge, H., Furuuchi, M., Hata, M., and Liu, X. G.: Chemical characteristics of size-resolved aerosols in winter in Beijing, J. Environ. Sci., 26, 1641–1650, 2014.

Sun, Y. L., Wang, Z. F., Fu, P. Q., Yang, T., Jiang, Q., Dong, H. B., Li, J., and Jia, J. J.: Aerosol composition, sources and processes during wintertime in Beijing, China, Atmos. Chem. Phys., 13, 4577–4592, doi:10.5194/acp-13-4577-2013, 2013.

Sun, Y. L., Jiang, Q., Wang, Z. F., Fu, P. Q., Li, J., Yang, T., and Yin, Y.: Investigation of the sources and evolution processes of severe haze pollution in Beijing in January 2013, J. Geophys. Res.-Atmos, 119, 4380–4398, doi:10.1002/2014jd021641, 2014.

Sun, Y. L., Wang, Z. F., Du, W., Zhang, Q., Wang, Q. Q., Fu, P. Q., Pan, X. L., Li, J., Jayne, J., and Worsnop, D. R.: Long-term real-time measurements of aerosol particle composition in Beijing, China: seasonal variations, meteorological effects, and source analysis, Atmos. Chem. Phys. Discuss., 15, 14549–14591, doi:10.5194/acpd-15-14549-2015, 2015.

Takegawa, N., Miyakawa, T., Kuwata, M., Kondo, Y., Zhao, Y., Han, S., Kita, K., Miyazaki, Y., Deng, Z., Xiao, R., Hu, M., van Pinxteren, D., Herrmann, H., Hofzumahaus, A., Holland, F., Wahner, A., Blake, D. R., Sugimoto, N., and Zhu, T.: Variability of submicron aerosol observed at a rural site in Beijing in the summer of 2006, J. Geophys. Res., 114, D00g05, doi:10.1029/2008jd010857, 2009.

Tang, G., Zhu, X., Hu, B., Xin, J., Wang, L., Münkel, C., Mao, G., and Wang, Y.: Vertical variations of aerosols and the effects responded to the emission control: application of lidar ceilometer in Beijing during APEC, 2014, Atmos. Chem. Phys. Discuss., 15, 13173–13209, doi:10.5194/acpd-15-13173-2015, 2015.

Tao, J., Ho, K. F., Chen, L. G., Zhu, L. H., Han, J. L., and Xu, Z. C.: Effect of chemical composition of $PM_{2.5}$ on visibility in Guangzhou, China, 2007 spring, Partic, 7, 68–75, doi:10.1016/j.partic.2008.11.002, 2009.

Tao, J., Zhang, L., Cao, J., Hsu, S.-C., Xia, X., Zhang, Z., Lin, Z., Cheng, T., and Zhang, R.: Characterization and source apportionment of aerosol light extinction in Chengdu, southwest China, Atmos. Environ., 95, 552–562, doi:10.1016/j.atmosenv.2014.07.017, 2014a.

ACPD
15, 33675–33730, 2015

Tao, J., Zhang, L., Ho, K., Zhang, R., Lin, Z., Zhang, Z., Lin, M., Cao, J., Liu, S., and Wang, G.: Impact of $PM_{2.5}$ chemical compositions on aerosol light scattering in Guangzhou-the largest megacity in South China, Atmos. Res., 135, 48–58, doi:10.1016/j.atmosres.2013.08.015, 2014b.

Tao, J., Zhang, L. M., Gao, J., Wang, H., Chai, F. H., Wang, S. L.: Aerosol chemical composition and light scattering during a winter season in Beijing, Atmos. Environ., 110, 36–44, doi:10.1016/j.atmosenv.2015.03.037, 2015.

Thompson, J. E., Hayes, P. L., Jimenez, J. L., Adachi, K., Zhang, X., Liu, J., Weber, R. J., and Buseck, P. R.: Aerosol optical properties at Pasadena, CA during CalNex 2010, Atmos. Environ., 55, 190–200, doi:10.1016/j.atmosenv.2012.03.011, 2012.

Titos, G., Foyo-Moreno, I., Lyamani, H., Querol, X., Alastuey, A., and Alados-Arboledas, L.: Optical properties and chemical composition of aerosol particles at an urban location: an estimation of the aerosol mass scattering and absorption efficiencies, J. Geophys. Res., 117, D04206, doi:10.1029/2011jd016671, 2012.

Turpin, B. J. and Lim, H. J.: Species contributions to $PM_{2.5}$ mass concentrations: revisiting common assumptions for estimating organic mass, Aerosol Sci. Tech., 35, 602–610, doi:10.1080/02786820119445, 2001.

Varma, R., Moosmüller, H., and Arnott, W. P.: Toward an ideal integrating nephelometer, Opt. Lett., 28, 1007–1009, 2003.

Wang, B., Li, K., Jin, W., Lu, Y., Zhang, Y., Shen, G., Wang, R., Shen, H., Li, W., Huang, Y., Zhang, Y., Wang, X., Li, X., Liu, W., Cao, H., and Tao, S.: Properties and inflammatory effects of various size fractions of ambient particulate matter from Beijing on A549 and J774 A.1 cells, Environ. Sci. Technol., 47, 10583–10590, doi:10.1021/es401394g, 2013.

Wang, X. F., Wang, T., Pathak, R. K., Hallquist, M., Gao, X. M., Nie, W., Xue, L. K., Gao, J., Gao, R., Zhang, Q. Z., Wang, W. X., Wang, S. L., Chai, F. H., and Chen, Y. Z.: Size distributions of aerosol sulfates and nitrates in Beijing during the 2008 Olympic Games: impacts of pollution control measures and regional transport, Adv. Atmos. Sci., 30, 341–353, 2013.

Wang, Y. H., Liu, Z. R., Zhang, J. K., Hu, B., Ji, D. S., Yu, Y. C., and Wang, Y. S.: Aerosol physicochemical properties and implications for visibility during an intense haze episode during winter in Beijing, Atmos. Chem. Phys., 15, 3205–3215, doi:10.5194/acp-15-3205-2015, 2015.

Watson, J. G.: Visibility: science and regulation, J. Air Waste Manage., 52, 628–713, 2002.

ACPD
15, 33675–33730, 2015

Wu, Q. Z., Wang, Z. F., Gbaguidi, A., Gao, C., Li, L. N., and Wang, W.: A numerical study of contributions to air pollution in Beijing during CAREBeijing-2006, Atmos. Chem. Phys., 11, 5997–6011, doi:10.5194/acp-11-5997-2011, 2011.

Wu, Z. J., Zheng, J., Shang, D. J., Du, Z. F., Wu, Y. S., Zeng, L. M., Wiedensohler, A., and Hu, M.: Particle hygroscopicity and its link to chemical composition in the urban atmosphere of Beijing, China during summertime, Atmos. Chem. Phys. Discuss., 15, 11495–11524, doi:10.5194/acpd-15-11495-2015, 2015.

Xu, J., Ma, J. Z., Zhang, X. L., Xu, X. B., Xu, X. F., Lin, W. L., Wang, Y., Meng, W., and Ma, Z. Q.: Measurements of ozone and its precursors in Beijing during summertime: impact of urban plumes on ozone pollution in downwind rural areas, Atmos. Chem. Phys., 11, 12241–12252, doi:10.5194/acp-11-12241-2011, 2011.

Xu, W. Q., Sun, Y. L., Chen, C., Du, W., Han, T. T., Wang, Q. Q., Fu, P. Q., Wang, Z. F., Zhao, X. J., Zhou, L. B., Ji, D. S., Wang, P. C., and Worsnop, D. R.: Aerosol composition, oxidative properties, and sources in Beijing: results from the 2014 Asia-Pacific Economic Cooperation Summit study, Atmos. Chem. Phys. Discuss., 15, 23407–23455, doi:10.5194/acpd-15-23407-2015, 2015.

Xu, X., Zhao, W., Wang, S., Zhang, Q., Qian, X., Fang, B., Venables, D. S., Chen, W., Gao, X., and Zhang, W.: Retrieval of the particulate complex refractive index by using cavity enhanced aerosol albedometer, in preparation, 2015.

Yan, P., Tang, J., Huang, J., Mao, J. T., Zhou, X. J., Liu, Q., Wang, Z. F., and Zhou, H. G.: The measurement of aerosol optical properties at a rural site in Northern China, Atmos. Chem. Phys., 8, 2229–2242, doi:10.5194/acp-8-2229-2008, 2008.

Yang, L. X., Wang, D. C., Cheng, S. H., Wang, Z., Zhou, Y., Zhou, X. H., and Wang, W. X.: Influence of meteorological conditions and particulate matter on visual range impairment in Jinan, China, Sci. Total Environ., 383, 164–173, doi:10.1016/j.scitotenv.2007.04.042, 2007.

Yang, Y. R., Liu, X. G., Qu, Y., An, J. L., Jiang, R., Zhang, Y. H., Sun, Y. L., Wu, Z. J., Zhang, F., Xu, W. Q., and Ma, Q. X.: Characteristics and formation mechanism of continuous hazes in China: a case study during the autumn of 2014 in the North China Plain, Atmos. Chem. Phys., 15, 8165–8178, doi:10.5194/acp-15-8165-2015, 2015.

Yao, T., Huang, X., He, L., Hu, M., Sun, T., Xue, L., Lin, Y., Zeng, L., and Zhang, Y.: High time resolution observation and statistical analysis of atmospheric light extinction properties and the chemical speciation of fine particulates, Sci. China Chem., 53, 1801–1808, doi:10.1007/s11426-010-4006-z, 2010.

ACPD
15, 33675–33730, 2015

Yu, Y., Dong, C., Wang, X., Yang, L., and Wang, W.: Size distributions of water-soluble inorganic ions of atmospheric aerosol particles in autumn in Jinan, China Environ. Sci., 4, 561–567, 2011.

Zhang, A., Qi, Q. W., Jiang, L. L., Zhou, F., and Wang, J. F.: Population exposure to $PM_{2.5}$ in the urban area of Beijing, PLoS One, 8, e63486, 2013.

Zhang, H., Hu, D., Chen, J., Ye, X., Wang, X., Hao, J., Wang, L., Zhang, R., and An, Z.: Particle size distribution and polycyclic aromatic hydrocarbons emissions from agricultural crop residue burning, Environ. Sci. Technol., 45, 5477–5482, 2011.

Zhang, X., Lin, Y. H., Surratt, J. D., and Weber, R. J.: Sources, composition and absorption Angstrom exponent of light-absorbing organic components in aerosol extracts from the Los Angeles Basin, Environ. Sci. Technol., 47, 3685–3693, doi:10.1021/es305047b, 2013.

Zhang, Y. H., Hu, M., Zhong, L. J., Wiedensohler, A., Liu, S. C., Andreae, M. O., Wang, W., and Fan, S. J.: Regional Integrated Experiments on Air Quality over Pearl River Delta 2004 (PRIDE-PRD2004): overview, Atmos. Environ., 42, 6157–6173, doi:10.1016/j.atmosenv.2008.03.025, 2008.

Zhao, W., Dong, M., Chen, W., Gu, X., Hu, C., Gao, X., Huang, W., and Zhang, W.: Wavelength-resolved optical extinction measurements of aerosols using broad-band cavity-enhanced absorption spectroscopy over the spectral range of 445–480 nm, Anal. Chem., 85, 2260–2268, doi:10.1021/ac303174n, 2013.

Zhao, W., Xu, X., Dong, M., Chen, W., Gu, X., Hu, C., Huang, Y., Gao, X., Huang, W., and Zhang, W.: Development of a cavity-enhanced aerosol albedometer, Atmos. Meas. Tech., 7, 2551–2566, doi:10.5194/amt-7-2551-2014, 2014.

Zhao, X. J., Zhao, P. S., Xu, J., Meng, W., Pu, W. W., Dong, F., He, D., and Shi, Q. F.: Analysis of a winter regional haze event and its formation mechanism in the North China Plain, Atmos. Chem. Phys., 13, 5685–5696, doi:10.5194/acp-13-5685-2013, 2013.

Zheng, G. J., Duan, F. K., Su, H., Ma, Y. L., Cheng, Y., Zheng, B., Zhang, Q., Huang, T., Kimoto, T., Chang, D., Pöschl, U., Cheng, Y. F., and He, K. B.: Exploring the severe winter haze in Beijing: the impact of synoptic weather, regional transport and heterogeneous reactions, Atmos. Chem. Phys., 15, 2969–2983, doi:10.5194/acp-15-2969-2015, 2015.

Zheng, S., Pozzer, A., Cao, C. X., and Lelieveld, J.: Long-term (2001–2012) concentrations of fine particulate matter ($PM_{2.5}$) and the impact on human health in Beijing, China, Atmos. Chem. Phys., 15, 5715–5725, doi:10.5194/acp-15-5715-2015, 2015.

ACPD
15, 33675–33730, 2015

Zhou, X. H., Gao, J., Wang, T., Wu, W. S., and Wang, W. X.: Measurment of black carbon aerosols near two Chinese megacities and the implications for improving emission inventories, Atmos. Environ., 43, 3918–3924, doi:10.1016/j.atmosenv.2009.03.062, 2009.

ACPD
15, 33675–33730, 2015

Table 1. List of the mean optical values (aerosol extinction, scattering, absorption coefficients, and SSA at $\lambda = 470\,\mathrm{nm}$), the effective mode diameters (particle number, surface area and volume, fitted values from the measured submicron size distribution with mono-lognormal distribution function), and chemical composition of $PM_{1.0}$ particles observed in this campaign. These parameters were classified into three different pollution levels (clear, slightly polluted and polluted days).

Parameter		Clear	Slightly Polluted	Polluted	All days
Optical	$\alpha_{ep,470}$ (Mm^{-1})	58.6 ± 81.6	186.7 ± 161.6	567.9 ± 292.3	200.9 ± 239.6
	$\alpha_{sp,470}$ (Mm^{-1})	47.2 ± 64.7	148.9 ± 131.9	477.2 ± 255.5	163.9 ± 201.7
	$\alpha_{ap,470}$ (Mm^{-1})	11.6 ± 18.3	37.8 ± 32.3	90.9 ± 55.8	37.0 ± 43.2
	ω_{470}	0.81 ± 0.10	0.79 ± 0.07	0.84 ± 0.06	0.80 ± 0.08
Size	$D_{p,n}$ (nm)	38 ± 31	73 ± 51	120 ± 64	67 ± 55
	$D_{p,s}$ (nm)	374 ± 130	338 ± 114	335 ± 76	351 ± 116
	$D_{p,v}$ (nm)	478 ± 94	480 ± 90	455 ± 82	475 ± 91
Chemical Composition ($\mu g\,m^{-3}$)	OC	3.41 ± 2.43	8.81 ± 4.64	20.47 ± 6.93	8.34 ± 6.97
	EC	0.48 ± 0.39	1.18 ± 0.59	2.72 ± 0.87	1.12 ± 0.92
	NO_3^-	1.78 ± 1.70	5.12 ± 3.56	14.99 ± 6.54	5.19 ± 5.52
	SO_4^{2-}	1.29 ± 0.69	3.20 ± 2.25	9.62 ± 4.55	3.35 ± 3.52
	NH_4^+	0.72 ± 0.75	2.98 ± 2.32	9.31 ± 4.33	2.98 ± 3.57
	Cl^-	0.52 ± 0.96	1.48 ± 1.41	4.46 ± 2.26	1.52 ± 1.88
	Ca^{2+}	0.31 ± 0.27	0.62 ± 0.38	0.58 ± 0.33	0.49 ± 0.36
	K^+	0.16 ± 0.25	0.50 ± 0.38	1.18 ± 0.46	0.46 ± 0.48
	Na^+	0.19 ± 0.22	0.33 ± 0.28	0.60 ± 0.38	0.32 ± 0.30
	Mg^{2+}	0.04 ± 0.03	0.08 ± 0.03	0.09 ± 0.03	0.06 ± 0.04

ACPD
15, 33675–33730, 2015

Table 2. List of aerosol mean diameters and optical properties during the selected haze episode.

Episode	Time (Data) (LT)	Number mean diameter (nm)	Surface mean diameter (nm)	$\alpha_{ep,470}$ (Mm^{-1})	$\alpha_{sp,470}$ (Mm^{-1})	$\alpha_{ap,470}$ (Mm^{-1})	ω_{470}	Real part of CRI (n)	Imaginary part of CRI (k)
Period 1	22 Nov 05:40–10:00	56 ± 6	193 ± 19	56 ± 24	44 ± 19	12 ± 6	0.79 ± 0.03	1.38 ± 0.06	0.03 ± 0.02
Period 2	22 Nov 12:40–15:00	25 ± 4	193 ± 17	17 ± 5	16 ± 5	1.0 ± 0.4	0.94 ± 0.03	1.40 ± 0.06	0.008 ± 0.005
Period 3	22 Nov 15:30–23 Nov 08:00	106 ± 16	229 ± 16	179 ± 69	151 ± 57	28 ± 12	0.85 ± 0.01	1.39 ± 0.04	0.02 ± 0.006
Period 4	23 Nov 08:30–12:00	105 ± 16	251 ± 15	405 ± 60	321 ± 42	84 ± 22	0.79 ± 0.03	1.40 ± 0.03	0.034 ± 0.008
Period 5	23 Nov 12:30–24 Nov 07:30	124 ± 19	263 ± 11	330 ± 110	283 ± 94	46 ± 16	0.86 ± 0.01	1.44 ± 0.03	0.02 ± 0.01
Period 6	24 Nov 08:00–11:10	80 ± 42	226 ± 14	80 ± 42	64 ± 34	16 ± 8	0.78 ± 0.04	1.40 ± 0.04	0.04 ± 0.02

ACPD
15, 33675–33730, 2015

Table 3. List of the mean values of aerosol scattering, absorption coefficients, and single scattering albedo in this campaign and recently reported values from references.

Location	Date (MM/yy)	λ (nm)	α_{sp} (Mm^{-1})	α_{ap} (Mm^{-1})	ω_0	RH	Inlet	References
Granada, Spain (Urban)	03/2006–02/2007	α_{sp}: 550 α_{ap}: 550	61 ± 25	24 ± 9	0.71 ± 0.07	< 50 %	PM_{10}	Titos et al. (2012)
Guangzhou (Urban)	07/2006	α_{sp}: 550 α_{ap}: 532	151 ± 103	34 ± 27	0.82 ± 0.07	< 40 %	PM_{10}	Garland et al. (2008)
Beijing (Urban)	01/2005–12/2006	α_{sp}: 525 α_{ap}: 532	255 ± 243	45 ± 39	0.80 ± 0.09	< 60 %	TSP	He et al. (2009)
Shanghai (Urban)	04–05/2010	α_{sp}: 532 α_{ap}: 532	102 ± 74	44 ± 35	0.70 ± 0.07	41.2 %	TSP	Li et al. (2013)
Xinken, PRD (Suburban)	10/2004–11/2004	α_{sp}: 550 α_{ap}: 630	333 ± 138	70 ± 42	0.83 ± 0.05	< 20 %	PM_{10}	Cheng et al. (2008)
Xianghe, Beijing (Suburban)	03/2005	α_{sp}: 550 α_{ap}: 550	468 ± 472	65 ± 75	0.81–0.85	< 42.5 %	TSP	Li et al. (2007)
Yufa, Beijing (Suburban)	08/2006–09/2006	α_{sp}: 550 α_{ap}: 532	361 ± 295	52 ± 37	0.86 ± 0.07	< 32 %	PM_{10}	Garland et al. (2009)
Huairou, Beijing (Suburban)	11/2014–01/2015	α_{sp}: 470 α_{ap}: 470	164 ± 202	37 ± 43	0.80 ± 0.08	< 15 %	$PM_{1.0}$	This work
Shangdianzi, Beijing (Rural)	09/2003–01/2005	α_{sp}: 525 α_{ap}: 525	175 ± 189	18 ± 13	0.88 ± 0.05	< 60 %	TSP	Yan et al. (2008)
Pasadena, US (Rural)	05/2010–06/2010	α_{sp}: 532 α_{ap}: 532	58 ± 43	4 ± 4	0.92 ± 0.08	< 50 %	$PM_{1.0}$	Thompson et al. (2012)

ACPD
15, 33675–33730, 2015

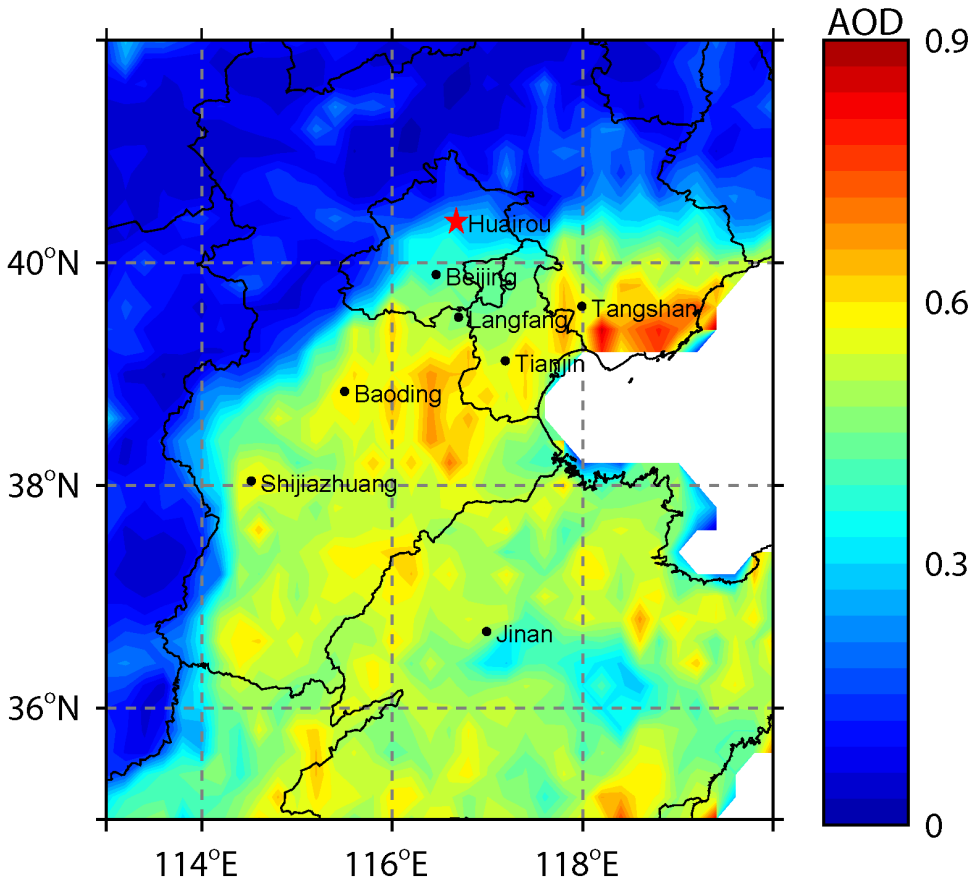

Figure 1. The map of the North China Plain. The observation site (Huairou) is marked with red star. The contour plot represents the average distribution of the MODIS AOD with 0.2° × 0.2° resolution during the campaign (16 November 2014 to 11 January 2015).

ACPD
15, 33675–33730, 2015

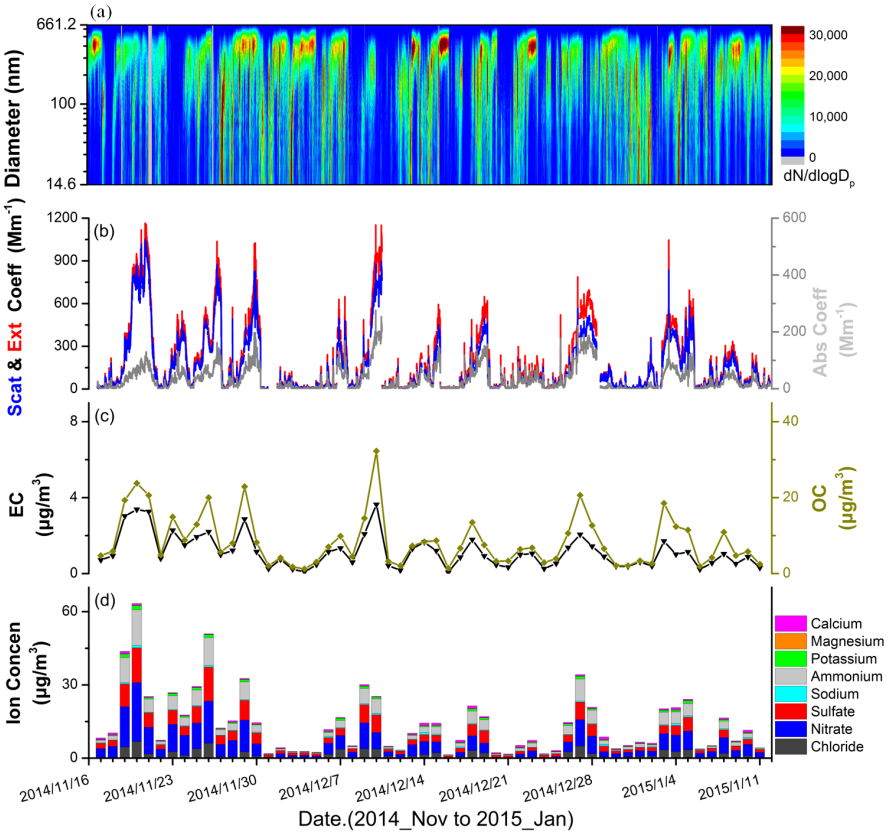

Figure 2. Time series of **(a)** the aerosol number size distribution measured by SMPS, **(b)** the extinction, scattering and absorption coefficients at $\lambda = 470$ nm measured by cavity enhanced albedometer, **(c)** organic carbon and element carbon concentration measured with an off-line aerosol carbon analyzer, and **(d)** water-insoluble ion concentrations measured with an off-line ion chromatography of dry $PM_{1.0}$ particles over the sampling period.

ACPD
15, 33675–33730, 2015

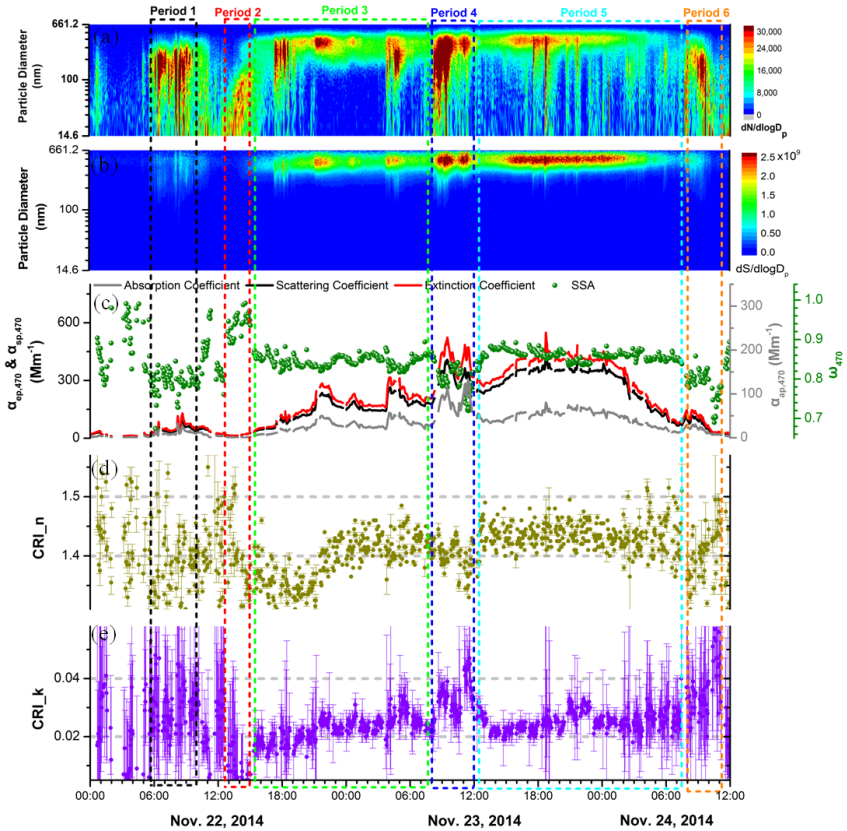

Figure 3. Highly time-resolved evolution of a selected air pollution episode during 22–24 November 2014. **(a)** Particle number size distribution, **(b)** particle surface size distribution, **(c)** aerosol extinction, scattering, absorption coefficients, and SSA at $\lambda = 470$ nm, **(d)** retrieved real part of CRI, **(e)** retrieved imaginary part of CRI. The air pollution episode was divided into six shorter periods to clearly show the evaluation of optical properties during haze formation, development and decline.

ACPD
15, 33675–33730, 2015

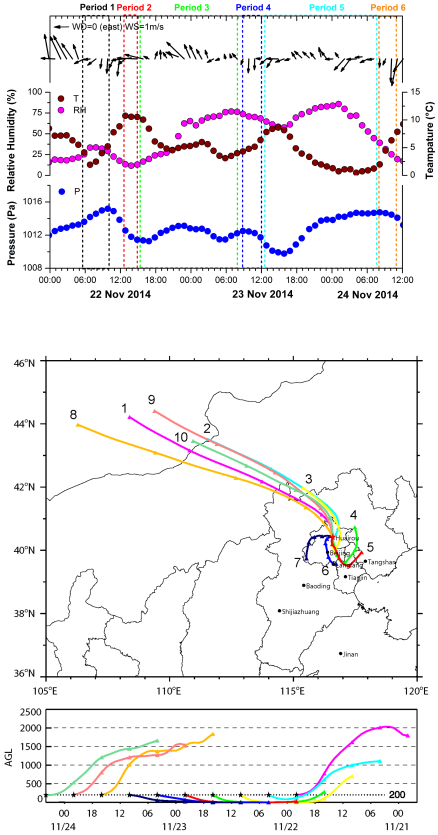

Figure 4. Upper panel: Temporal wind direction and speed, temperature, relative humidity and pressure of atmosphere air. Six different periods (the same as in Fig. 3) represent the evolution of the optical properties with different aerosol processes. Lower panel: The 24 h back trajectories starting at 200 m a.g.l. in Huairou site were calculated every 6 h (at 00:00, 06:00, 12:00 and 18:00 LT) during the selected air pollution episode.

ACPD
15, 33675–33730, 2015

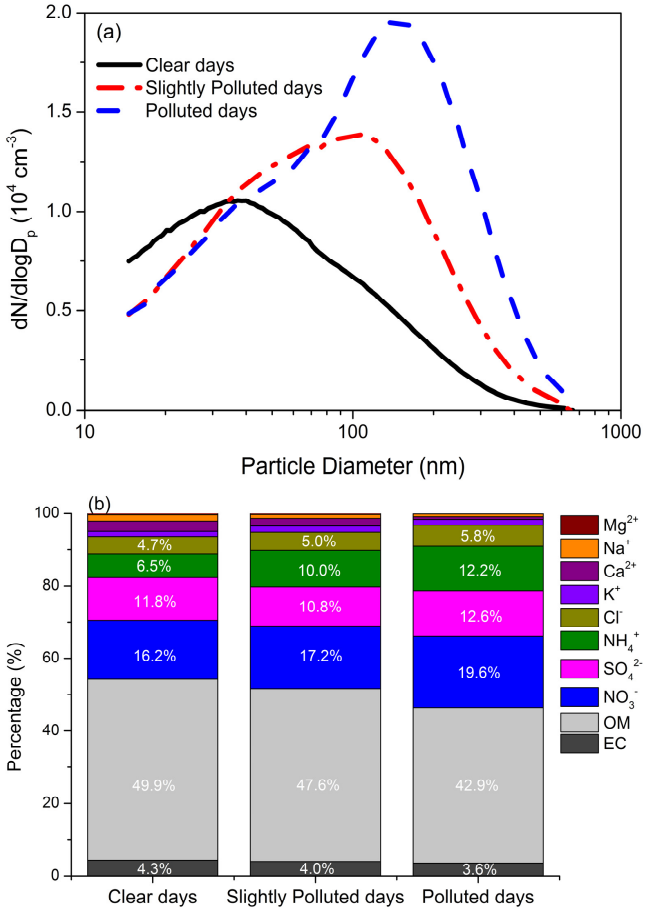

Figure 5. (a) The mean number size distribution and **(b)** percentage contribution of OM, EC concentrations and 8 water-soluble ion compositions on clear, slightly polluted and polluted days.

ACPD
15, 33675–33730, 2015

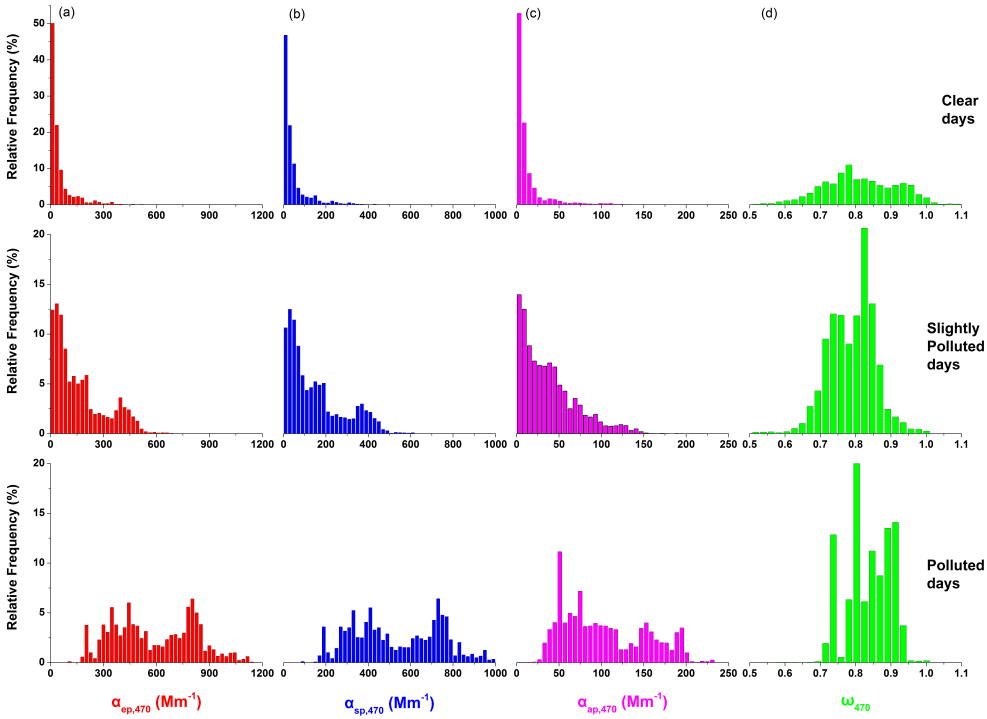

Figure 6. The frequency distributions of dry $PM_{1.0}$ optical properties at $\lambda = 470$ nm observed during the campaign. **(a)** Extinction coefficient, **(b)** scattering coefficient, **(c)** absorption coefficient, **(d)** single scattering albedo on clear, slightly polluted and polluted days.

ACPD
15, 33675–33730, 2015

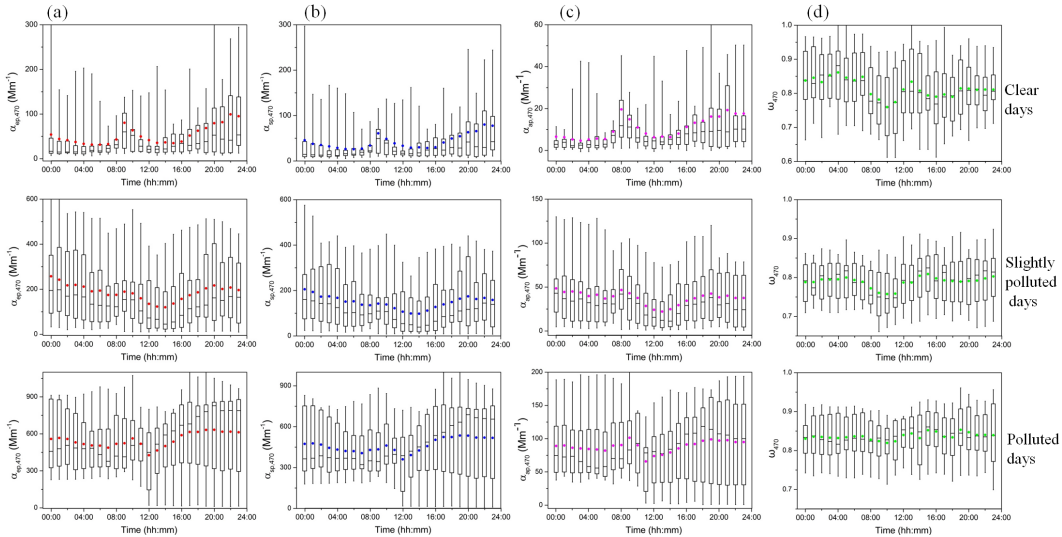

Figure 7. Diurnal variations of hourly averaged **(a)** extinction coefficient, **(b)** scattering coefficient, **(c)** absorption coefficient and **(d)** SSA at $\lambda = 470$ nm on clear, slightly polluted and polluted days. The error bars are 5th and 95th percentiles and the limits of the boxes represent 25th and 75th percentiles.

ACPD
15, 33675–33730, 2015

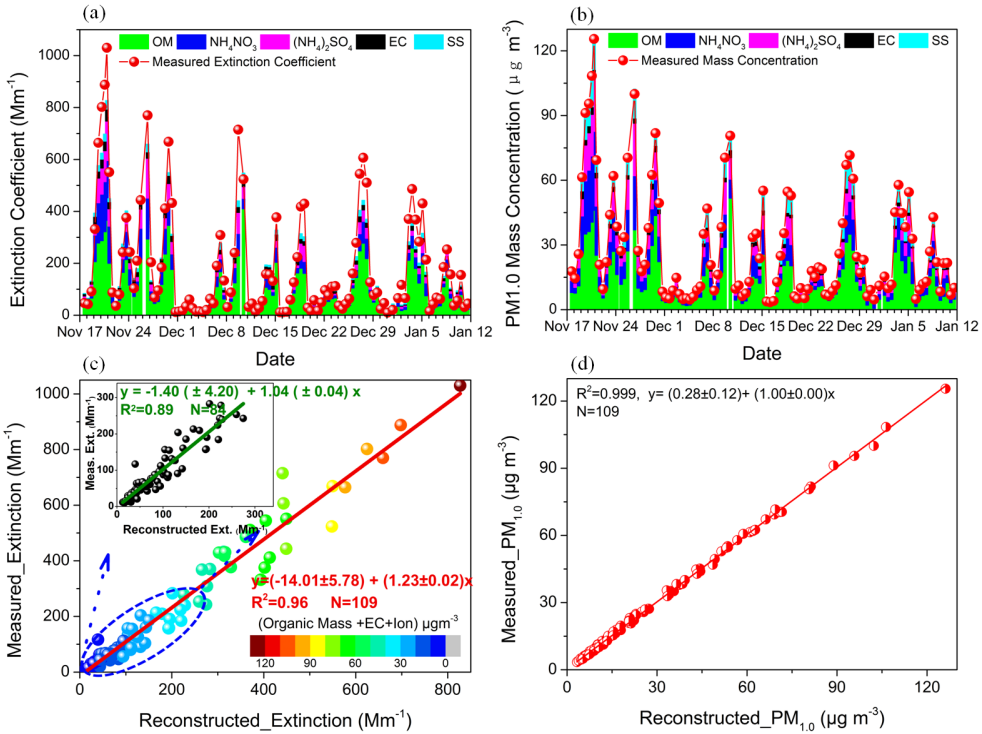

Figure 8. (a) and **(b)**: The plot of measured and reconstruction value of the extinction and mass concentration, respectively; **(c)** and **(d)**: Scatter plot of the measured extinction coefficient at $\lambda = 470$ nm and $PM_{1.0}$ mass concentration against the reconstructed values with the modified IMPROVE formula. Insert of panel **(c)** shows the linear regression between measured and reconstructed extinction coefficient under lower aerosol load condition (with extinction smaller than 300 Mm^{-1}).

ACPD
15, 33675–33730, 2015

Optical properties of atmospheric fine particles near Beijing during the HOPE-J^{3}A Campaign

X. Xu et al.

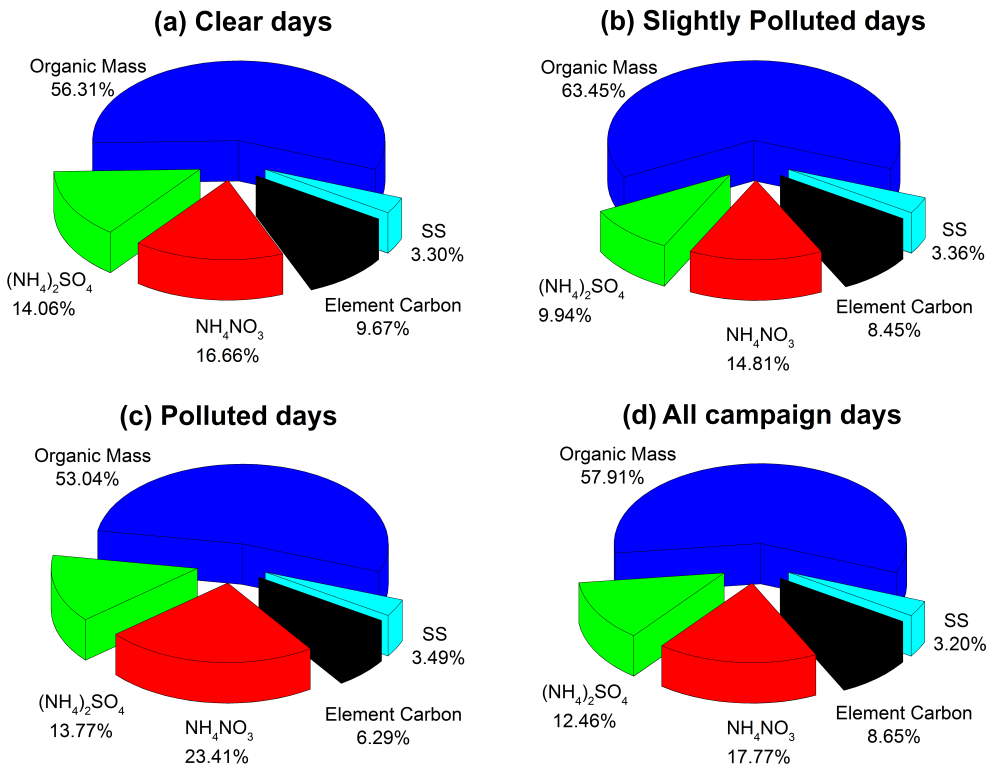

Figure 9. Average fractional contribution of each chemical composition to dry $PM_{1.0}$ extinction coefficient with respect to different pollution level.

ACPD
15, 33675–33730, 2015

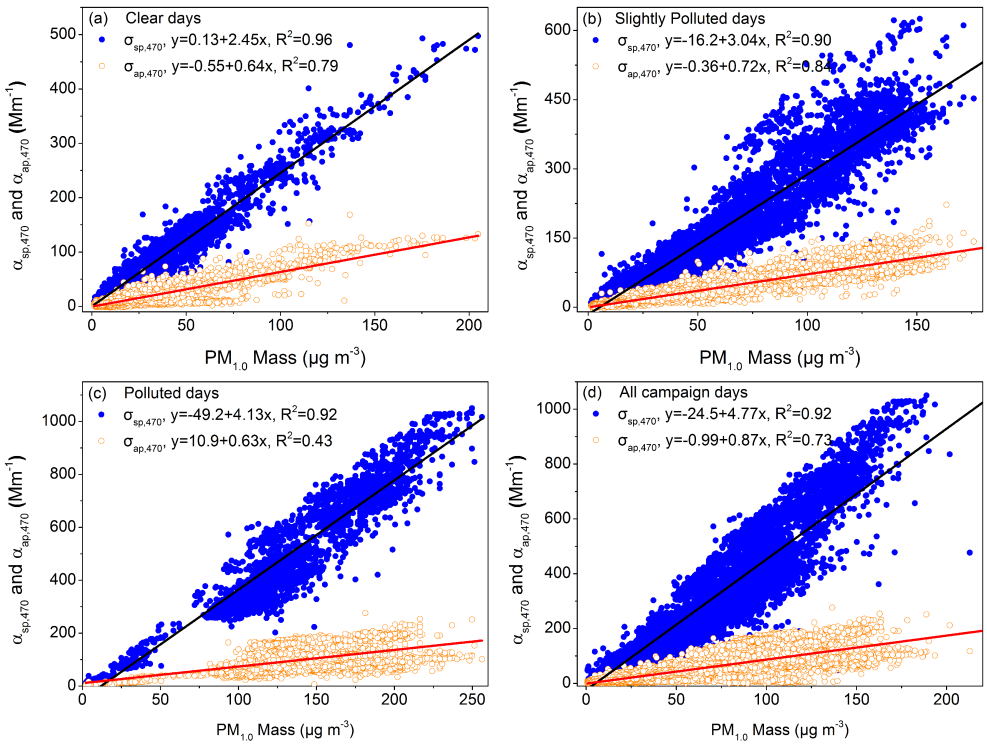

Figure 10. Scatter plots of the measured scattering and absorption coefficients at $\lambda = 470$ nm against $PM_{1.0}$ mass concentrations for $PM_{1.0}$ particles under different pollution level.

ACPD
15, 33675–33730, 2015

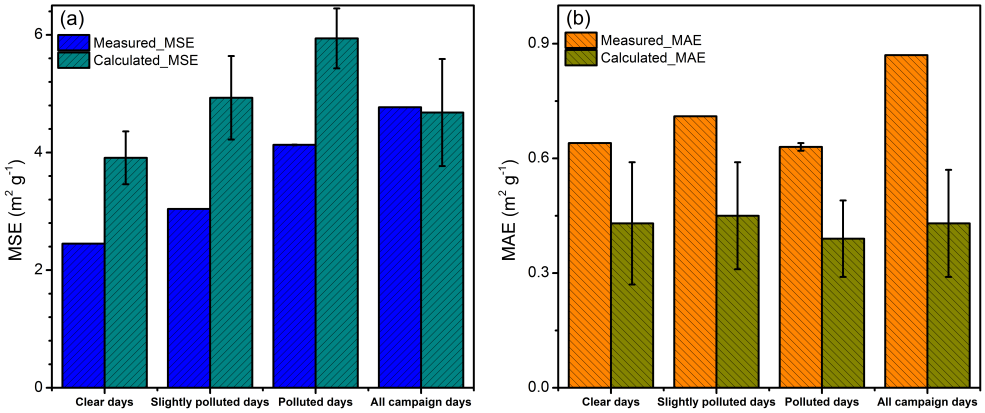

Figure 11. Comparisons of measured and reconstructed **(a)** MSE and **(b)** MAE of $PM_{1.0}$ particles under different pollution level.

ACPD
15, 33675–33730, 2015